Available online at www.sciencedirect.com
SCIENCE DIRECT®
Coordination Chemistry Reviews 249 (2005) 457–483
COORDINATION CHEMISTRY REVIEWS
www.elsevier.com/locate/ccr

Review

Exited state electron and energy transfer in molecular assemblies

My Hang V. Huynh[a], Dana M. Dattelbaum[a], Thomas J. Meyer[b,*]

[a] *Dynamic Experimentations Division, DX-2: Materials and Dynamics Group, MS C920, Los Alamos National Laboratory, Los Alamos, NM 87545, USA*
[b] *Associate Director Strategic Research, MS A127, Los Alamos National Laboratory, Los Alamos, NM 87545, USA*

Received 2 April 2004; accepted 6 July 2004
Available online 22 September 2004

This article is dedicated to Henry Taube. He was the Ph.D. supervisor of one of the authors of this account (TJM) and an inspiration to a generation of chemists. His elucidation of the basic principles of electron transfer combined with the theoretical contributions by R.A. Marcus and N.S. Hush set the stage for a new understanding of chemical reactivity.

Contents

Abstract

The metal-to-ligand charge transfer (MLCT) excited states of polypyridyl complexes of the d^6 ions Ru(II), Os(II), and Re(I) have provided the basis for many studies on photochemical electron and energy transfer. In this account, a brief review of photochemical electron transfer by $[Ru(bpy)_3]^{2+*}$ is given, followed by an update on MLCT excited state molecular and electronic structure, and an introduction to photochemical electron and energy transfer in molecular assemblies. The majority of the account is devoted to describing the evolution of two approaches to preparing complex molecular assemblies for the study of photochemical electron and energy transfer both inspired by the demands of achieving artificial photosynthesis. The first approach involves the derivatization of preformed polystyrene by added chromophores and electron or energy transfer donors or acceptors and three generations of polymers differing in polymer content and linkage strategies. The second approach has exploited solid-state peptide synthesis and the stepwise preparation of oligopeptides with spatial control of added groups and alignment on the resulting helical scaffolds.

Keywords: Metal-to-ligand charge transfer; Excited state; Photophysics; Electron transfer; Energy transfer; Artificial photosynthesis; Molecular assemblies; Polystyrene; Polymers; Oligopeptides

* Corresponding author. Tel.: +1 505 667 3762; fax: +1 505 667 0500.
E-mail address: tjmeyer@lanl.gov (T.J. Meyer).

0010-8545/$ – see front matter © 2004 Elsevier B.V. All rights reserved.
doi:10.1016/j.ccr.2004.07.005

1. Introduction

In the early 1970s, it was shown that metal complex excited states could undergo electron-transfer [1–10]. The first experiments involved $[Ru(bpy)_3]^{2+}$ (bpy is 2,2′-bipyridine) which has a lowest energy metal-to-ligand charge transfer (MLCT) excited state 2.1 eV above the ground state, Eq. (1):

$$[Ru^{II}(bpy)_3]^{2+} \xrightarrow{+h\nu} [Ru^{III}(bpy^-)(bpy)_2]^{2*} \quad (1)$$

Redox potentials for the oxidation and reduction of both ground and excited state couples for this complex are shown in Scheme 1 in CH_3CN (I = 0.1 M) versus the saturated sodium chloride calomel reference electrode (SSCE). The excited state values were initially estimated by using a kinetic quenching technique [11,12].

The data in Scheme 1 show that the excited state is a stronger oxidant and reductant than the ground state by the 2.1 eV energy of the excited state. The implied ability of the excited state to undergo electron transfer was demonstrated by a series of flash photolysis experiments in the presence of electron transfer quenchers such as the methyviologen dication (MV^{2+}; $E°(MV^{2+/+})$ = −0.6 V versus SSCE) and 10-methylphenothiazine (10-MePTZ; $E°(MePTZ^{+/0})$ = 0.73 V). The appearance of the electron transfer products was shown by direct spectral observation following flash photolysis [3–6,10–19].

In the example in Scheme 2 [4], visible Ru^{II*} → bpy MLCT excitation and relaxation gives the excited state

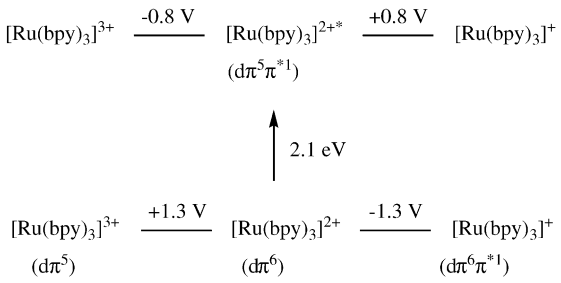

Scheme 1. Excited and ground state redox potentials.

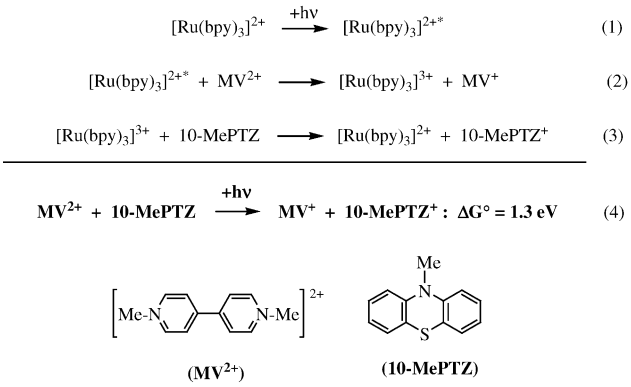

Scheme 2. Light-to-chemical energy conversion by excited state electron transfer.

$[Ru(bpy)_3]^{2+*}$. With appropriate concentrations of added MV^{2+} and 10-MePTZ, $[Ru(bpy)_3]^{2+*}$ undergoes first diffusional, oxidative quenching by MV^{2+} to give $[Ru(bpy)_3]^{3+}$ and MV^+ in a reaction favored by $\Delta G° = -0.2$ eV. The oxidized complex is subsequently reduced by10-MePTZ with $\Delta G° = -0.5$ eV.

The net effect of the excitation-electron transfer sequence is to use visible light to drive a chemical reaction uphill with the transient storage of 1.3 eV of chemical energy. These were important early observations since they pointed to a new approach to the conversion of light to chemical energy and the basis for a new field, artificial photosynthesis [20–22].

The reaction in Scheme 1 is carried out in solution, and there is no directional sense to the coupled excitation-electron transfer sequence. Following the excitation-electron transfer sequence, back electron transfer converts the transiently stored chemical redox energy into heat. There is no molecular basis for utilizing or storing the energy created in the excitation-electron transfer sequence.

The goals of artificial photosynthesis are to use excited state electron transfer chemistry to achieve solar energy conversion by producing a photopotential and associated current or to drive high-energy reactions such as the splitting of water into H_2 and $(1/2)O_2$. There may also be applications in green chemistry and the use of visible light to carry out synthetically important reactions such as the epoxidation of olefins, Eq. (2).

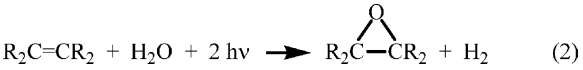

For molecular systems to be used in such applications, the excitation-electron transfer apparatus must be incorporated into ordered arrays. The arrays need to be constructed so that directed (vectorial) electron transfer can occur away from the site at which photochemical oxidative and reductive equivalents are produced driven by free energy gradients [23–27].

An additional requirement for water splitting, or light-to-chemical energy conversion in general, is creation of an electron transfer interface to catalytic sites where oxidation and reduction can occur. These are the sites where photochemical oxidative and reductive equivalents drive separate oxidative and reductive half reactions. The target half reactions for water splitting are shown in Scheme 3 and for the reduction of carbon dioxide by water to give formic acid and hydrogen in

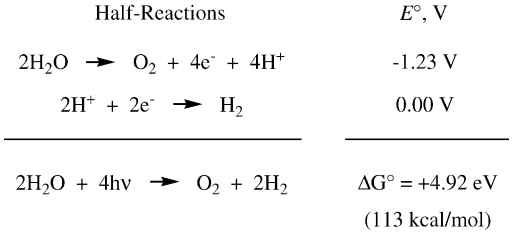

Scheme 3. Thermodynamics for water splitting.

Eq. (3).

$$2H_2O + CO_2 + 4h\nu \rightarrow O_2 + 2HCO_2H,$$
$$\Delta G^\circ = +6.52\,\text{eV} \quad (h\nu < 760\,\text{nm}) \qquad (3)$$

With this goal in mind, the Meyer research group embarked on a series of studies designed to create catalysts for water oxidation [28,29] and CO_2 reduction [30,31]. The focus was on molecules that upon chemical or electrochemical oxidation or reduction would oxidize water or reduce CO_2. With this strategy, a successful molecular catalyst would be subsequently incorporated into a larger molecular array and linked to a vectorial excitation-electron transfer apparatus. In this approach, it was necessary to take the linkage chemistry into account from the beginning.

The work on catalysts was productive. A series of metal complexes were identified which electrocatalytically reduced CO_2 [30,31]. The blue dimer, *cis*,*cis*-$[(bpy)_2(H_2O)Ru^{III}–O–Ru^{III}(H_2O)(bpy)_2]^{4+}$, was shown to be a water oxidation catalyst, and its mechanism for water oxidation was studied in detail [28,29,32].

A molecular block diagram showing the essential functional elements required for light-to-chemical conversion in a single molecular array is shown below, Fig. 1. It includes a light absorption-antenna apparatus, a chromophore site sensitized by the antenna, a donor–acceptor electron transfer array, and molecular catalysts for oxidation ($Red_2 \rightarrow Ox_2$) and reduction ($Ox_1 \rightarrow Red_1$). Although the design and construction of such an array is a daunting task, the success of green plants in utilizing photosystems I and II for water oxidation and CO_2 reduction was both noteworthy and inspirational [33,34].

In order to assemble, the required components in spatially controlled molecular arrays required an underlying molecular architecture, a general linkage chemistry, and the synthetic flexibility required to make systematic modifications. The remainder of this account is largely devoted to describing the evolution of two different approaches to this problem. One is based on the derivatization of preformed polystyrene and the other the stepwise, solid-state peptide synthesis of oligoprolines.

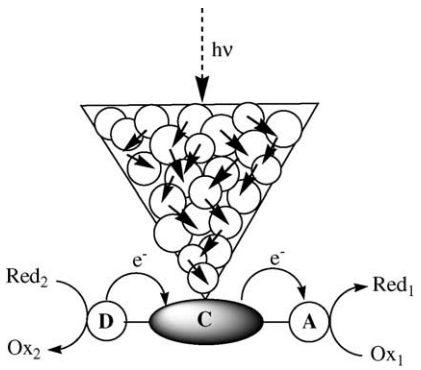

Fig. 1. Reaction center model.

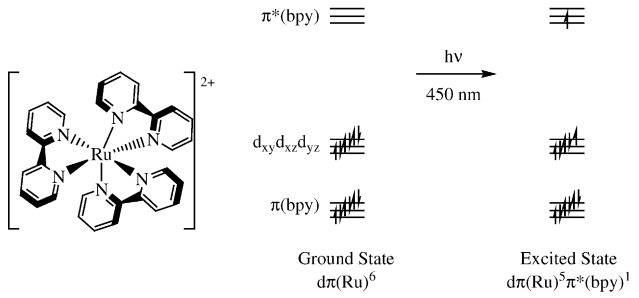

Fig. 2. Schematic energy level diagram showing the ground and lowest MLCT excited state(s) of $[Ru(bpy)_3]^{2+}$.

It is useful first to discuss recent results on MLCT excited states and then to give a brief account of photochemical electron and energy transfer in molecular assemblies based on polypyridyl complexes of Ru and Os.

2. Metal-to-ligand charge transfer (MLCT) excited states

The parent molecule for molecular assemblies based on polypyridyl complexes is $[Ru(bpy)_3]^{2+}$. Its ground and lowest metal-to-ligand charge transfer (MLCT) excited state electronic structures and the optical transition that interconverts them are illustrated in Fig. 2. The lowest excited state is a triplet state split into a manifold of three states separated by $\sim$100 cm^{-1} by low symmetry and spin–orbit coupling.

A great deal is known about MLCT excited states. They dominate the spectroscopy, photochemistry, and photophysics of polypyridyl complexes of Ru(II), Os(II), and Re(I) [35–38]. The pulsed laser techniques transient resonance Raman (TR^3), transient infrared (TRIR), and, more recently, transient near infrared (TRNIR) have been very useful in acquiring information about excited state electronic and molecular structure and have been successfully applied to MLCT excited states [39–43].

A block diagram of the apparatus that we have used for acquiring TRIR and TRNIR spectra is shown in Fig. 3. It is based on a Bruker IFS 66 V/s FTIR spectrometer. Signal-time profiles are obtained at a fixed mirror setting with the FT

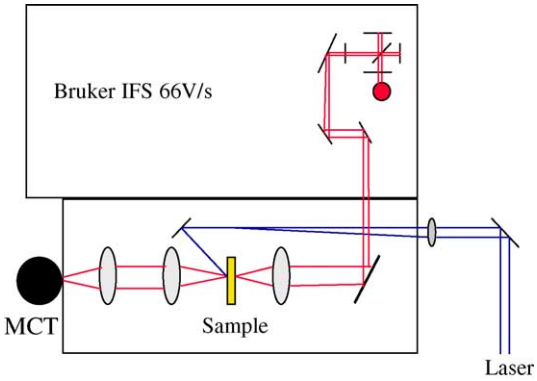

Fig. 3. Block diagram of the transient near infrared (TRNIR) spectrometer.

spectrum acquired by scanning the mirror positions, and the final spectrum obtained from the Fourier transforms. The spectral region of interest, infrared or near infrared, is accessed by changing the beam splitters and sources [44].

Application of the TRIR technique allowed a clear resolution to a vexing question. Is the MLCT excited state of $[Ru(bpy)_3]^{2+}$ localized with the excited electron occupying a single bpy ligand, $[Ru^{III}(bpy^{\bullet -})(bpy)_2]^{2+*}$, or is it delocalized with the excited electron delocalized over all three, $[Ru^{III}(bpy^{1/3\bullet -})_3]^{2+*}$? Both are possible. There is a direct analogy with ground state mixed-valence molecules, where both localized and delocalized examples are known, and there are examples of molecules in a transition region which have some of the properties of each [45].

In $[Ru(bpy)_3]^{2+*}$, the mixed valency is ligand-based with the metal acting as an intervening "bridge". Based on an analysis of the localized-to-delocalized transition in mixed-valence molecules, the key parameters are the magnitude of the resonance energy arising from bpy–$bpy^{\bullet -}$ electronic coupling, H_{DA}, and the sum of the intramolecular (λ_i) and solvent (λ_o) reorganization energies. The excited state would be delocalized if $2|H_{DA}| > \lambda$ and localized if $2|H_{DA}| < \lambda$ [45–48].

In the excited state infrared spectrum of $[Ru(bpy)_3]^{2+*}$ in the ν(bpy) ring stretching region in CD_3CN from 1400 to 1500 cm^{-1}, two sets of bands appear. Bands typical of ground state bpy appear at ν(bpy) = 1425, 1447, 1466, 1487, and 1604 cm^{-1} and for $bpy^{\bullet -}$, at 1418, 1446, 1465, 1488, and 1541 cm^{-1}. The appearance of both sets of bands proves that the excited electron is localized on one ligand in the thermally equilibrated excited state on the nanosecond time scale [49]. This result is consistent with results from earlier TR^3 measurements [50].

Although the excited electron is localized, ultrafast absorption polarization measurements by Papanikolas and coworkers [51] and Kelly and coworkers [52,53] reveal that it hops from ligand to ligand on the tens of ps time scale for $[Ru(bpy)_3]^{2+*}$ and with τ = 8.7 ps for $[Os(bpy)_3]^{2+*}$ [51]. The movement of the electron associated with the polarization changes has been described as inter-ligand electron transfer (ILET), but a more appropriate description is given below.

The lowest energy process leading to inter-ligand electron transfer is illustrated in Scheme 4 for $[Os(phen)_3]^{2+*}$. An electron is transferred from the lowest π^* level on phen ligand a ($\pi^*_{1,a}$) to the lowest level on ligand b ($\pi^*_{1,b}$). In this lowest energy process, electron transfer is accompanied by hole transfer from $d\pi_3$ to $d\pi_1$. The initial hole in $d\pi_3$ is aligned along the reduced ligand axis and bpy_a which maximizes the electron–hole electrostatic interaction. Both electron and hole are transferred in the lowest energy pathway leading to ILET. Because there are three low-lying MLCT states both initially and finally, there are actually nine separate transitions contributing to the change in polarization. Transfer of the electron without transfer of the hole gives an upper MLCT excited state with the hole in $d\pi_3$ or $d\pi_2$ rather than in $d\pi_1$. In related Os(III) polypyridyl ground state complexes, the energies of the higher energy MLCT excited states, ΔE_1 and ΔE_2 in Fig. 4, are ~4000 cm^{-1} and ~6000 cm^{-1} above the lowest state [45].

There is an equivalent, degenerate process in which the electron is transferred from $\pi^*_{1,a}$ to the lowest π^* level on ligand c, $\pi^*_{1,c}$ and hole transfer to $d\pi_2$. Rather than ILET, which occurs in singly reduced $[Ru(bpy)_3]^+$ with no hole in the $d\pi^6$ core, these processes are more appropriately described as thermally activated transitions between degenerate MLCT states, MLCT(1) → MLCT(2), MLCT(3) [54]. They have also been described as intramolecular excitonic transitions [55]. They have the effect of rotating the excited state dipole around the molecule which explains the time dependent polarization changes observed in the ultrafast polarization measurements.

In the TRNIR spectrum of $[Os(phen)_3]^{2+*}$ in CD_3CN, a new absorption band appears at $\bar{\nu}_{max}$ = 4980 cm^{-1} with $\Delta\bar{\nu}_{1/2}$ = 2200 cm^{-1}, Fig. 4. Within experimental error, this transient

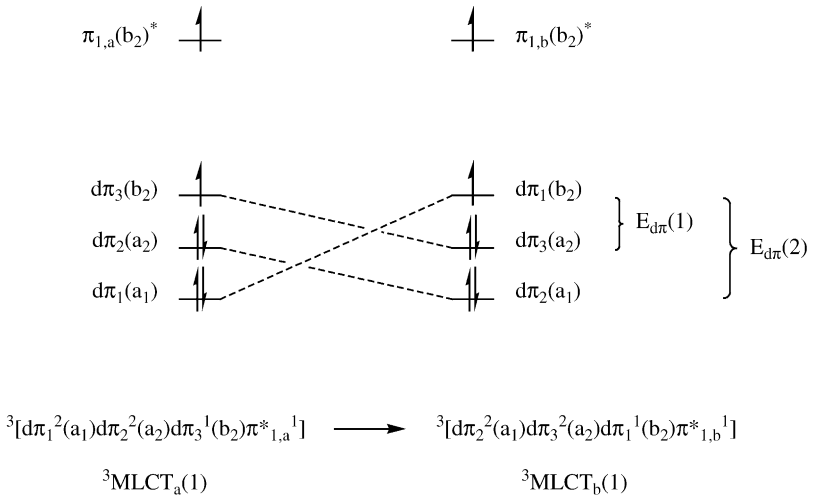

Scheme 4. Changes in electronic configuration for the lowest energy pathway for inter-ligand electron transfer (ILET) illustrating the simultaneous transfer of both electron and hole.

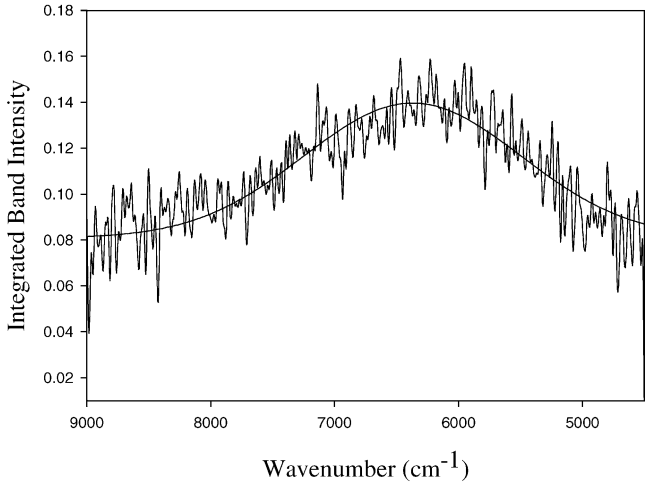

Fig. 4. The low energy absorption band for $[Os(phen)_3]^{2+*}$.

feature decays with the lifetime of the MLCT excited state, τ = 120 ns (k = 8.3 × 10^6 s^{-1}) as measured independently by transient emission measurements. It has been assigned to the spectroscopic analog of the degenerate, thermally activated MLCT(1) → MLCT(2), MLCT(3) processes that lead to changes in excited state polarization. The band is solvent dependent consistent with the change in spatial orientation of the excited state dipole accompanying the transition [54].

The spectroscopic MLCT → MLCT transition gains intensity from the low symmetry of the excited state and spin–orbit coupling. They have the effect of mixing the three-dπ orbitals in the $d\pi^5$ excited state core. A similar band is observed for $[Ru(bpy)_3]^{2+*}$ at ∼4500 cm^{-1}, but it is of considerably lower intensity. The lower intensity is expected since there is less coupling between the degenerate MLCT excited states given the lower spin–orbit coupling constant for Ru(III) (∼1000 cm^{-1}) compared to Os(III) (∼3000 cm^{-1}).

The observation of thermally activated processes that interrelate degenerate or nearly degenerate MLCT excited states on the ps to tens of ps time scale may be important in explaining excited state dynamics. Internal reorientation of the MLCT excited state dipole from an initially excited polypyridyl ligand may be required to facilitate electron or energy transfer to an appended quencher on another ligand. On the other hand, inter-ligand electron transfer without transfer of the associated hole is not a viable mechanism for redistributing the excited electron on short time scales. Electron-transfer without hole transfer is a high-energy activated process since it creates an upper MLCT excited state.

3. Photochemical electron and energy transfer in ligand-bridged and chromophore–quencher assemblies

The demonstration of excited state electron transfer in solution and the need to control its directionality led to the design of polypyridyl complexes derivatized by appending electron or energy transfer donors or acceptors. The phrase chromophore–quencher complex was coined to describe these complexes. The goal was to duplicate the excitation-electron transfer sequence in Scheme 2 but in a single molecular unit without a requirement for diffusion. Synthetically, this entailed either linking complexes by ligand bridges or by linking groups to polypyridyl ligands. This imposed limitations on the thermodynamic acceptor or donor properties of the added electron or energy transfer groups in order to achieve the internal free energy gradients required to direct electron or energy transfer along specific molecular directions.

In early experiments, both synthetic approaches were explored with examples cited in references [23–25,56–59,62]. This work has been reviewed [22,60,61] including insights into chemical approaches to artificial photosynthesis and how to couple sequential excitation-electron transfer with chemical catalysis of redox reactions [20–22,26].

An early product of this strategy, a collaborative effort with the research group of Mike Elliott at Colorado State, is shown in Fig. 5 [62,63]. It contains derivatives of methylviologen dication and 10-methylphenothiazine, used in Scheme 2, linked to separate bpy ligands by methylene (–CH_2–) spacers.

The donor-chromophore–acceptor complex in Fig. 5 is actually one of four positional isomers which differ with regard to the relative dispositions of the appended viologen and phenothiazine groups [63]. As shown by laser flash photolysis in CH_3CN at room temperature, MLCT excita-

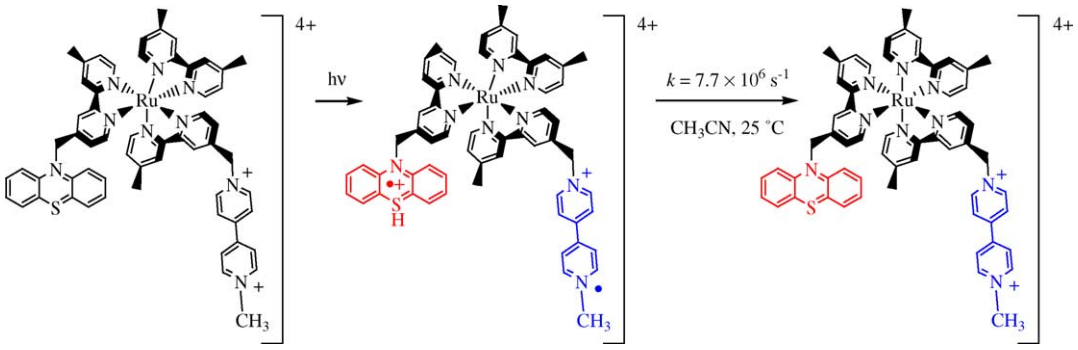

Fig. 5. Structure of a chromophore–quencher donor–chromophore-acceptor complex.

tion is followed by excited state electron transfer to the appended viologen which occurs with $k \sim 6 \times 10^{10}\,s^{-1}$ ($\tau \sim 16$ ps) in a model complex [64]. This is the same time scale as energy transfer to a bpy-appended anthracene, see below, [65] and more rapid than rotation of the excited state dipole by MLCT → MLCT interconversion in $[Ru(bpy)_3]^{2+*}$ [52,53]. It is slow on the sub-ps time scale for internal relaxation to the lowest triplet state(s) following MLCT excitation of $[Ru(bpy)_3]^{2+*}$ as shown by ultrafast transient absorption measurements [66,67].

The initial quenching event is followed by rapid PTZ → Ru(III) electron transfer, which occurs with $k \sim 1 \times 10^{10}\,s^{-1}$, to give the redox-separated (RS) state shown in Fig. 5. This state has chemically linked reduced ($-MV^{\bullet+}$) and oxidized ($-PTZ^{\bullet+}$) groups separated by methylene spacers. $-MV^{\bullet+} \rightarrow -PTZ^{\bullet+}$ back electron transfer returns the RS state to the ground state and is favored by $\Delta G^\circ = -1.14$ eV. The rate constant for back electron transfer varies in the range $k = (4.5–7.7) \times 10^6\,s^{-1}$ depending on the isomer [63].

Back electron transfer occurs in the inverted region. The defining feature of the inverted region is that the driving force for electron transfer (ΔG°) is greater than the sum of the solvent and intramolecular reorganization energies ($\lambda = \lambda_i + \lambda_o$) with $|\Delta G^\circ| > \lambda$. $|\Delta G^\circ| > \lambda$ for both electron transfer in the inverted region and nonradiative decay of excited states, e.g., $[Ru(bpy)_3]^{2+*}$. The two differ in that in a RS state, the electron transfer donor and acceptor are well separated spatially and weakly coupled electronically. In an excited state, there is strong electronic coupling [68–70]. In comparing the two, there is a direct analogy with the localized and delocalized limits in mixed-valence chemistry [45].

Intramolecular energy transfer has been similarly demonstrated in Ru-bpy complexes containing appended energy transfer acceptors such as anthracene [65,71–73]. A recent example studied by ultrafast spectroscopy is $[Ru(dmb)_2(bpy\text{-}An)]^{2+}$ (dmb is 4,4′-Me_2-2,2′-bipyridine) which contains an anthracene group appended to bpy by a $-CH_2CH_2-$ spacer, Fig. 6. By using dmb as the remaining ligands, each of the three bpy acceptor ligands is nearly equivalent electronically [65].

Fast transient spectroscopic measurements in CH_3CN at room temperature reveal the presence of two transients. The slower ($\tau = 27$ ps, $k = 3.7 \times 10^{10}\,s^{-1}$) was attributed to ILET, or more appropriately, MLCT → MLCT, Eq. (4), and the faster ($\tau = 16$ ps, $k = 6.2 \times 10^{10}\,s^{-1}$) to direct MLCT → An energy transfer following excitation at the bpy-An ligand.

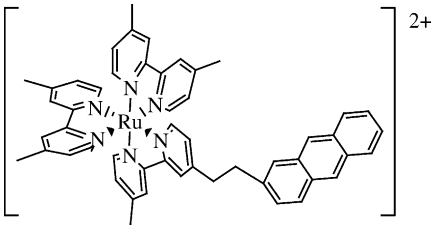

Fig. 6. Structure of the chromophore–energy transfer quencher complex.

MLCT → An energy transfer is favored by $\Delta G^\circ = -0.3$ eV [65].

$$[Ru^{III}(dmb^{\bullet-})(dmb)(bpy\text{-}An)]^{2+*} \rightarrow [Ru^{III}(dmb)_2(bpy^{\bullet-}\text{-}An)]^{2+*} \quad (4)$$

$$[Ru^{III}(dmb)_2(bpy^{\bullet-}\text{-}An)]^{2+*} \rightarrow [Ru(dmb)_2(bpy\text{-}{}^3An^*)]^{2+} \quad (5)$$

The TRNIR technique has also been applied to the observation of intervalence transfer (IT) in the MLCT excited state of a ligand-bridged complex [74]. One-electron oxidation of $[(tpy)Ru^{II}(tppz)Ru^{II}(tpy)]^{4+}$ (tpy = 2,2′:6′,2″-terpyridine, tppz is 2,3,5,6-tetrakis(2-pyridyl)pyrazine) gives the corresponding Ru(III)–Ru(II) mixed-valence ion, Scheme 5 [74–79]. The structures of the tpy and tppz ligands are also shown in Scheme 5. The lowest lying π* acceptor level is on the tppz bridging ligand. In $[(tpy)Ru^{II}(tppz)Ru^{II}(tpy)]^{4+}$ a low energy, intense Ru(II) → tppz band appears at $\lambda_{max} = 548$ nm ($\varepsilon = 2.4 \times 10^4\,M^{-1}\,cm^{-1}$). In the mixed-valence ion, an IT band appears at $\bar{\nu}_{max} = 6550\,cm^{-1}$ ($\lambda_{max} = 1530$ nm) in CD_3CN.

As shown at the bottom of Scheme 5, visible Ru(II) → tpy,tppz MLCT excitation of $[(tpy)Ru^{II}(tppz)Ru^{II}(tpy)]^{4+}$ creates a mixed-valence, MLCT excited state with the excited electron in the lowest π* level of the bridging ligand. From transient absorption measurements $\tau \sim 80$ ns ($k = 1.2 \times 10^7\,s^{-1}$) which is within the time window of the TRNIR spectrometer shown in Fig. 3. This raises the possibility of observing an IT band in the excited state (bottom, Scheme 5). This would allow a comparison to be made between neutral (tppz) and radical anion ($tppz^{\bullet-}$) as mixed-valence bridging ligands.

In the TRNIR spectrum of the excited state, a band appears at $\bar{\nu}_{max} = 6300\,cm^{-1}$ ($\lambda_{max} = 1590$ nm) which decays with the lifetime of the MLCT excited state. It has been assigned to the IT transition in Scheme 5 which allows a comparison to be made between the excited and ground state IT spectra. In CD_3CN at 298 K, $\bar{\nu}_{max} = 6550\,cm^{-1}$ ($\Delta\bar{\nu}_{1/2} = 970\,cm^{-1}$, $\varepsilon_{max} = 7560\,M^{-1}\,cm^{-1}$) for the ground state and $\bar{\nu}_{max} = 6300\,cm^{-1}$ ($\Delta\bar{\nu}_{1/2} = 1070\,cm^{-1}$, $\varepsilon_{max} = 3300\,M^{-1}\,cm^{-1}$) for the excited state.

The similarity in band shapes shows that the extent of solvent and intramolecular vibrational coupling to the Ru(II) → Ru(III) IT transition is comparable for both tppz and $tppz^{\bullet-}$ as bridging ligands. In the localized, classical limit the energy of the IT band is given by $E_{IT} = \lambda = \lambda_i + \lambda_o$. The band intensity is higher by ∼2 for the ground state pointing to more extensive metal–metal coupling through $d\pi(Ru^{II})$–π*(tppz) mixing than through π*($tppz^{\bullet-}$)–$d\pi(Ru^{III})$ mixing.

A detailed interpretation is complicated by the fact that three IT bands are predicted in both the ground and excited state spectra. They arise from transitions from each of the three dπ levels at Ru(II) ($d\pi_1$, $d\pi_2$, $d\pi_3$) to the hole in $d\pi_3$

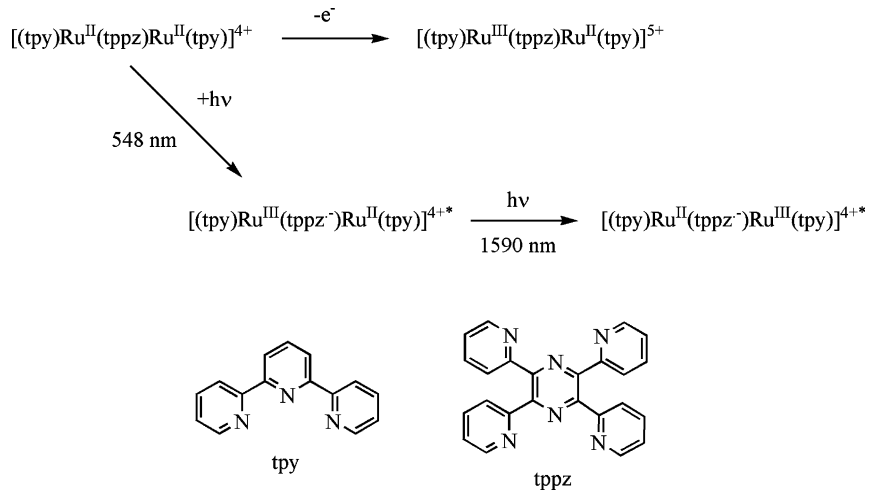

Scheme 5. The mixed-valence MLCT excited state of $[(tpy)Ru^{II}(tppz)Ru^{II}(tpy)]^{4+}$.

at Ru(III) [45]. The band observed in the ground state, and by inference in the excited state, appears to be two overlapping bands arising from the higher lying IT transitions $d\pi_2(Ru(II)_a)$, $d\pi_3(Ru(II)_a) \rightarrow d\pi_3(Ru(III)_b)$ [80].

An excited state IT band has also been observed for the pyz-based MLCT excited state *cis*,*cis*-$[(bpy)_2(Cl)Ru^{III}(pz^{\bullet -})Ru^{II}(Cl)(bpy)_2]^{2+*}$ (pyz is pyrazine) at $\bar{\nu}_{max} = 6880\,cm^{-1}$ with $\Delta\bar{\nu}_{1/2} = 3740\,cm^{-1}$. In this case, the TRNIR measurements were conducted with the complex in a free standing polymethymethacrylate (PMMA) film. The rigid medium provided by the film was required because of the photochemical instability of the complex in solution toward ligand loss [81].

4. Molecular assemblies based on derivatized polystyrene

Building more complex assemblies, which incorporate the minimum set of components required for artificial photosynthesis, requires a molecular scaffold that can be easily derivatized. We initially chose polystyrene, in part, because the electronic structure of the styryl repeat units ensures that this scaffold is relatively inert toward electron or energy transfer. There are no low-lying excited states, and oxidation or reduction occurs at high oxidative or low reductive potentials.

There is an extensive background literature for preparing polystyrene samples having known, reproducible molecular weight distributions by using free radical or living radical anion initiation techniques. Polystyrene offers considerable synthetic flexibility with regard to linkage chemistry based on known reactions of added functional groups. By using controlled synthetic conditions, it is possible to add more than one functional group to individual polymer strands in sequential, stepwise reactions and so to control content. A disadvantage is that unless block copolymers are used; it is not possible to control the relative spatial positions of sequentially added functional groups.

There is a growing literature of derivatized soluble polymers as scaffolds for the study of photochemical electron and energy transfer [82–96]. Our work in this area began in the 1980s initially with Ru(II) polypyridyl complexes bound to poly-4-vinylpyridine [97]. We then evolved a linkage strategy to polystyrene based on the derivatization of a 1:1 styrene–chloromethylstyrene copolymer by chloride displacement.

4.1. Copolymers of styrene–m,p-chloromethylstyrene

The polymer used in early studies was a 1:1 copolymer of styrene and a mixture of *meta*- and *para*-chloromethylstyrenes. It was prepared by free radical polymerization with AIBN (azobis-isobutyronitrile) as the initiator. Standard conditions are available for preparing this polymer in various molecular weight ranges [98]. In one of the first experiments, a polymer was prepared with the number average molecular weight $M_n = 7800$. This corresponds to, on the average, ~30 styrene–chloromethylstyrene repeat units. The average number of repeat units is defined as the ratio of M_n to the formula weight of the repeat unit. Free radical initiation results in samples with relatively broad molecular weight distributions typically with polydispersities (the ratio of the mass average molecular weight to the number average molecular weight; M_w/M_n) greater than 2. Derivatized forms of the polymer were prepared with partial loading of individual strands by displacement of Cl^- by phenothiazine anion, the monomethylated precursor to MV^{2+}, and the mono-deprotonated form of the complex $[Ru(bpy)_2(4,4'-(CO_2H)_2bpy)]^{2+}$.

In an initial photochemical experiment, the events in Scheme 2 were repeated, but in solutions containing $[Ru(bpy)_3]^{2+}$ and the MV^{2+} and phenothiazine electron transfer acceptors and donors linked to separate polymer

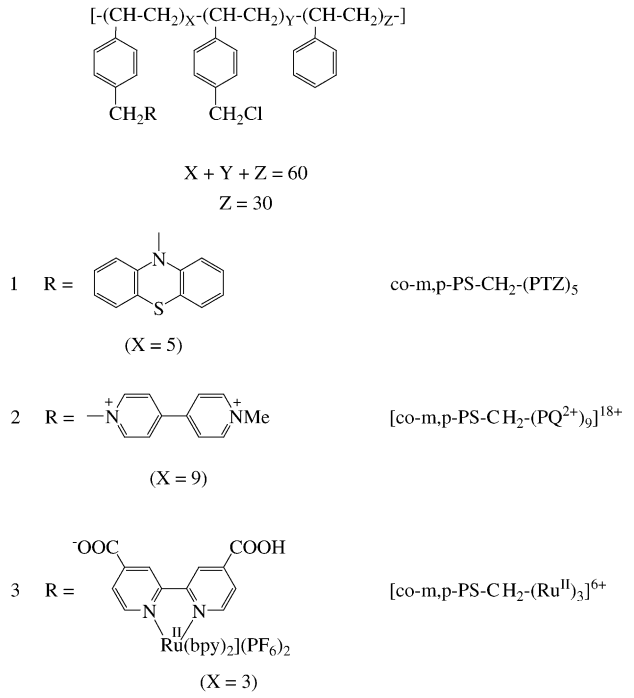

Scheme 6. Structures and abbreviations for the chromophore and redox polymers.

strands. Polymer binding greatly decreases diffusional mobilities. In solutions containing $[Ru(bpy)_3]^{2+}$ and the derivatized MV^{2+} and phenothiazine polymers, excitation, quenching, and electron transfer result in the appearance of $MV^{\bullet+}$ and $MV^{\bullet 2+}$ on separate polymer strands. The striking result was that the time scale for subsequent $MV^{\bullet+}$ + $PTZ^{\bullet+}$ back electron transfer was slower on the polymers by a factor of ~500 [99,100].

In a subsequent experiment, a complex electron and energy transfer shuttling scheme was demonstrated in solutions containing $[Ru(bpy)_3]^{2+}$ and the same electron transfer donor–acceptor pair all on separate strands [106]. The partly loaded samples and a generic structural formula for the derivatized polymers are shown in Scheme 6.

In acidified DMF solutions containing [co-*m*,*p*-PS-CH_2-$(PTS)_5$], [co-*m*,*p*-PS-CH_2-$(PQ^{2+})_9]^{18+}$, and [co-*m*,*p*-PS-CH_2-$(Ru^{II})_3]^{6+}$, $Ru^{II} \rightarrow$ bpy MLCT excitation results in no excited state quenching at low added polymer concentrations because of the polymer-induced inhibition to diffusion. The abbreviations used for the polymers reflect the 1:1 copolymer, define the chemical link to the polymer, and give the extent of loading out of ~30 available sites.

Excited state quenching does occur in the same solution following addition of 9-methylanthracene (9-MeAn, 0.42 mg/ml). Quenching is accompanied by the appearance of $PTZ^{\bullet+}$ and $MV^{\bullet+}$ on separate polymer strands as shown by laser flash photolysis.

These measurements were used to demonstrate the sequence of reactions shown in Scheme 7. In this sequence, 9-MeAn plays a dual role as both energy and electron transfer relay. The initial step (reaction 1 in Scheme 7) involves

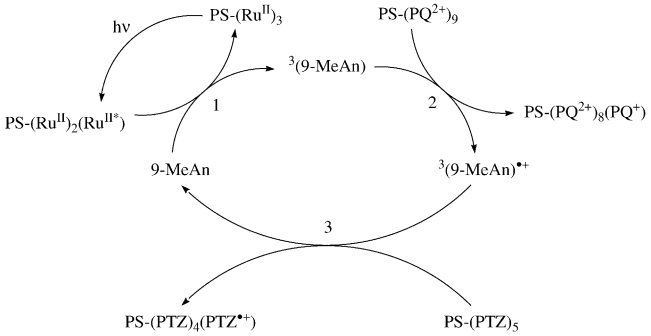

Scheme 7. Use of 9-MeAn as both energy and electron transfer relay.

diffusional quenching of Ru(II)* by 9-MeAn in [co-*m*,*p*-PS-CH_2-$(Ru^{II})_3]^{6+}$ to give the anthracene triplet ^{3}(9-MeAn) at 1.8 eV. Once formed, ^{3}(9-MeAn) diffuses to [co-*m*,*p*-PS-CH_2-$(PQ^{2+})_9]^{18+}$ where it undergoes electron transfer (reaction 2) with $\Delta G^\circ \sim -0.9$ eV. In the last step, the anthracene cation, $(9\text{-MeAn})^+$, undergoes electron transfer with [co-*m*,*p*-PS-CH_2-$(PTZ)_5$] to give polymer-linked PTZ^+ in a reaction favored by $\Delta G^\circ = -0.3$ eV [101].

The time scale for back electron transfer between polymer-bound $PTZ^{\bullet+}$ and $PQ^{\bullet+}$ on separate polymer strands was increased by a factor of 27 compared to back electron transfer between untethered $PTZ^{\bullet+}$ and $PQ^{\bullet+}$ under the same conditions. Once again, this was due to the decreased mobility of the $MV^{\bullet+}$ and $PTZ^{\bullet+}$ groups localized on separate polymer strands [101].

4.2. Ether links to 1:1 poly-styrene–p-chloromethylstyrene

In a subsequent series of experiments, a 1:1 styrene–*p*-chloromethylstyrene copolymer was used in which only the *p*-isomer of chloromethylstyrene was present. Free radical polymerization gave atactic polymer samples of varying number average molecular weights and polydispersities depending on the reaction conditions [102–104].

With this polymer, a new linkage chemistry was developed for the polypyridyl complexes based on chloride displacement by the alcohol derivatives $[M(bpy)_2(bpyCH_2OH)]^{2+}$ (M = Ru, Os; $bpyCH_2OH$ = 4-Me-4′CH_2OH-2,2′-bipyridine) in the presence of CsOH in DMSO [102–104]. The extent of polymer loading was controlled by using the complex as the limiting reagent. More complex assemblies were prepared by subsequent nucleophilic displacement of all or part of the remaining chloro sites on the polymer backbone. A repeat unit of a polymer containing the Ru(II) complex is shown as structure (3) in Fig. 7.

Fig. 8 illustrates two of the many low-energy conformations of the polymer [co-PS-CH_2OCH_2-$(Ru^{II})_{30}]^{60+}$. These are calculated structures with the metal complexes included as spheres of diameter 14 Å represented by the open spheres in Fig. 8. The underlying carbon skeleton of the polymer backbone can be seen in the structure. The relatively large

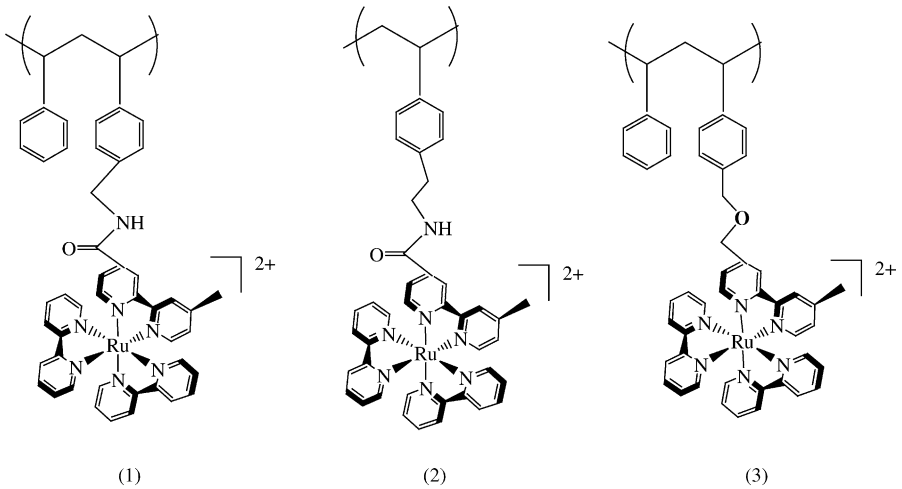

Fig. 7. Repeat units of the polymers [co-PS-$CH_2NHC(O)$-$(Ru^{II})_n$)]$^{2n+}$ (1), [PS-$CH_2CH_2NHC(O)$-$(Ru^{II})_n$]$^{2n+}$ (2), and [co-PSCH_2OCH_2-$(Ru^{II})_n$)]$^{2n+}$ (3).

size of the cationic complexes enforces a spatially extended structure on the polymer array. The periphery-to-periphery distance between nearest neighbors is 7 ± 2 Å and between non-nearest neighbors 20 ± 6 Å [105].

The 1:1 styrene–*para*-chloromethylstyrene co-polymers provided a systematic means for preparing polymers containing both pendant polypyridyl complexes and electron or energy transfer donors or acceptors [102,104,105]. The modified polymers were used to demonstrate intra and intermolecular electron and energy transfer [101,105,106], energy and electron transfer shuttling by a bifunctional polymer containing both appended anthracene and PTZ [106], and the build up of multiple redox equivalents on single polymeric strands [107]. A review of early work in this area was published in Coordination Chemistry Reviews in 1991 [105].

Multi-electron, multi-photon photochemistry was also demonstrated in an ether-linked Ru(II) homo polymer. In these experiments, [co-PS-CH_2OCH_2-$(Ru^{II})_{30}$]$(PF_6)_{60}$ was excited by visible laser flash excitation in CH_3CN in the presence of relatively high concentrations of PTZ and the extent of $PTZ^{\bullet+}$ formation observed as a function of incident laser irradiance. At high irradiances, multiple excitation and quenching led to individual polymeric strands that were reduced, on the average, by up to seven electrons, Eq. (6) [108].

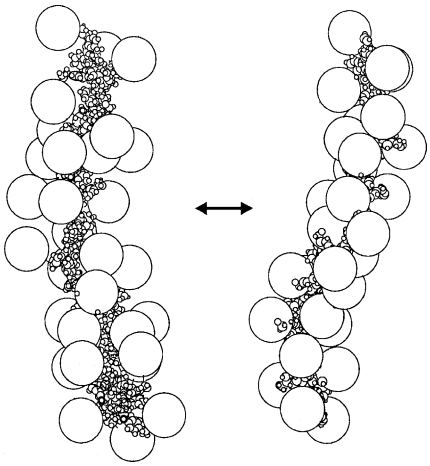

Fig. 8. Two of the many low energy conformers for the polymer [co-$PSCH_2OCH_2$-$(Ru^{II})_{30}$]$^{60+}$ with the complex shown as the open spheres of diameter 14 Å.

$$[\text{co-PS-CH}_2\text{OCH}_2\text{-(Ru(II))}_{30}]^{60+} + 7h\nu + 7\text{PTZ} \rightarrow [\text{co-PS-CH}_2\text{OCH}_2\text{-(Ru(II))}_{23}(\text{Ru(II)})_7]^{53+} + 7\text{PTZ}^{\bullet+} \quad (6)$$

An important issue for energy conversion was to establish whether the polymers could undergo facile intra-strand electron and energy transfer. This would allow light absorption followed by the channeling of redox or excited state equivalents to a remote site or sites where chemical energy conversion could occur.

This point was explored in the mixed Ru(II)–Os(II) polymer [co-PS-CH_2OCH_2-$(Ru^{II})_{22}(Os^{II})_5$]$(PF_6)_{54}$ in which Os(II) can act as a "trap" site with $Ru^{II*} \rightarrow Os^{II}$ energy transfer favored by $\Delta G^\circ = -0.36$ eV. Transient emission measurements in CH_3CN showed that rapid ($k > 2 \times 10^8$ s^{-1}) $Ru^{II*} \rightarrow Os^{II}$ energy transfer occurs but only at Ru(II) sites adjacent to Os(II) [103]. The excited state properties of Ru(II)* sites on polymer samples dilute in Ru(II) were essentially unperturbed and superimposable on those of the model complex $[Ru(bpy)_2(bpy)\text{-}CH_2OH]^{2+}$. In the fully loaded homo polymer [co-PS-CH_2OCH_2-$(Ru^{II})_{30}$]$(PF_6)_{60}$, excited state decay is non-exponential because of multi-photon polarization effects. When a second excited state is created near a first, changes in local polarization in the solvent and polymer create a different local environment which results in a distribution of decay times [105,110].

Possible pathways for intrastrand energy transfer are shown in Scheme 8. Reactions (ii) and (iii) show that $Ru^{II*} \rightarrow Os^{II}$ energy transfer following excitation at Ru(II) sites (open spheres) without adjacent Os(II) trap sites (hatched spheres) requires $Ru^{II*} \rightarrow Ru^{II}$ energy migration. Long-range Ru^{II*}

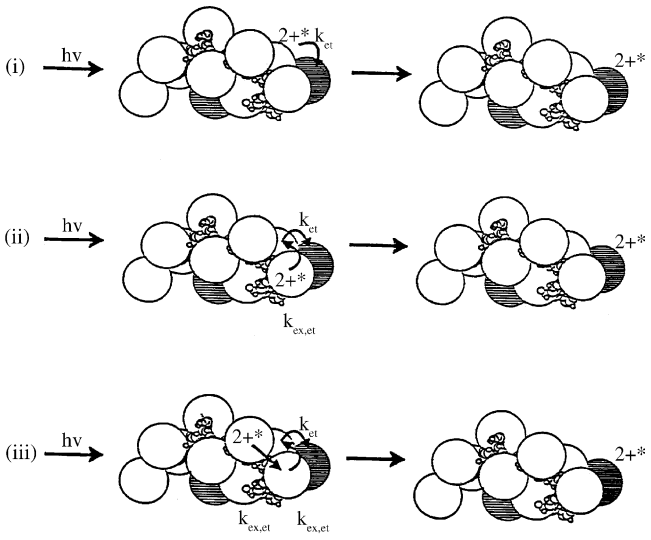

Scheme 8. Pathways for intra-strand energy migration and transfer. The open spheres are Ru(II) and the cross-hatched spheres the Os(II) quencher.

$\rightarrow Os^{II}$ energy transfer is unlikely to be competitive because of the 21 ± 6 Å distance between second-nearest neighbors. As shown in reaction (iii), migration to an Os(II) trap site could require more than one migration step followed by $Ru^{II*} \rightarrow Os^{II}$ energy transfer, reaction (i).

The transient decay data show that energy migration is relatively slow with $\tau > 1000$ ns ($k < 1 \times 10^6\ s^{-1}$). Slow energy migration relative to the excited state lifetime of the Ru(II)* carrier, $\tau = 810$ ns ($k = 1.2 \times 10^6\ s^{-1}$), rules out the ether-linked polymers as candidates for molecular-level antenna arrays. Energy migration by $Ru^{II*} \rightarrow Ru^{II}$ energy transfer hopping is too slow [103,105].

Hole migration by $Ru^{III} \leftarrow Ru^{II}$ electron transfer was investigated in the same polymer by adding an irreversible, oxidative quencher, the diazonium salt [*p*-$CH_3OC_6H_4N_2$]BF_4 (35 mM). MLCT excitation at sites removed from Os(II) was followed by irreversible oxidative quenching, Eq. (7).

$$[PS\text{-}(Ru^{II})_{21}(Ru^{II*})(Os^{II})_5]^{60+} + ArN_2{}^{+} \rightarrow [PS\text{-}(Ru^{II})_{21}(Ru^{III})(Os^{II})_5]^{61+} + ArN_2 \quad (7)$$

The diazonium radical formed in the quenching reaction decomposes irreversibly by coupling or loss of N_2 and extraction of $H^{\bullet}$ from the solvent. The Ru(III) site undergoes intra-strand $Ru^{III} \leftarrow Ru^{II}$ electron transfer "self exchange" by site-to-site migration until the hole is delivered to a Ru(II) site adjacent to Os(II) where rapid $Os^{II} \rightarrow Ru^{III}$ electron transfer occurs with $\Delta G^{\circ} = -0.41$ eV. Analysis of the laser flash photolysis results in CH_3CN at 298 K gave k(295, μ = 0.035 M) = (5.3 ± 0.9) × $10^6\ s^{-1}$ for the migration rate constant [103].

$$-Ru(III) - Ru(II) - Os(II) - \rightarrow -Ru(II) - Ru(III) - Os(II) - \rightarrow -Ru(II) - Ru(II) - Os(III) - \quad (k_{mig}) \quad (8)$$

Intra-strand energy migration and transfer was shown to occur in a triply functionalized polymer containing Ru(II), Os(II), and derivatized 9-methoxy anthracene. In the partly loaded polymer [co-PS-CH_2OCH_2-$(Ru^{II})_3(Os^{II})_3$]$(PF_6)_{12}$ with only 6 of, on the average, 30 sites derivatized, there was no evidence for $Ru^{II*} \rightarrow Os^{II}$ energy transfer following excitation at Ru(II). Emission quantum yields and excited state lifetimes for Ru^{II*} and Os^{II*} were essentially the same as in equivalent homo polymers containing the separate Ru(II) or Os(II) chromophores at the same loading level [102].

In [co-PS-CH_2OCH_2-$(Ru^{II})_3(An)_6$]$(PF_6)_6$, which is lightly loaded in complex, $Ru^{II*} \rightarrow$ An quenching does occur with $k = 7.6 \times 10^6\ s^{-1}$ in 1,2-dichloroethane. Quenching is viscosity dependent, and the energy transfer mechanism appears to involve local segmental rotations and intra-strand coiling to bring Ru^{II*} into physical or near-physical contact with An. In [co-PS-CH_2OCH_2-$(Ru^{II})_3(An)_{21}$]$(PF_6)_6$, each Ru(II) site is adjacent to an anthracene, and quenching is rapid with $k > 2 \times 10^8\ s^{-1}$ [105,107].

The absence of quenching in [co-PS-CH_2OCH_2-$(Ru^{II})_3(Os^{II})_3$]$(PF_6)_{12}$ points to M(II) sites spread along individual polymeric strands with the higher M(II) content inhibiting intra-strand coiling. Reaction of the unreacted chloro sites with an excess of 9-$HOCH_2$-anthracene in the presence of CsOH in DMSO gave the triply derivatized polymer [co-PS-CH_2OCH_2-$(Ru^{II})_3(An)_{17}(Os^{II})_3$]$(PF_6)_{12}$.

As shown in Scheme 9, the added anthracene provides an excited state of intermediate energy (^{3}An at 1.8 eV) which intervenes spatially between the Ru(II) and Os(II) sites distributed along the polymer backbone. Following excitation at Ru(II), efficient $Ru^{II*} \rightarrow Os^{II}$ energy transfer occurs. In the mechanism in Scheme 9, $Ru^{II*} \rightarrow$ An energy transfer quenching (k_q in Scheme 9), ^{3}An → An energy migration (k_{mig}), and ^{3}An → Os^{II} energy transfer (k_{en}) are all rapid with $k > 1 \times 10^8\ s^{-1}$ in 1,2-dichloroethane at 298 K [102].

In a significant fraction of the photochemical events, energy is transported over long distances by ^{3}An → An migration. The net effect is that anthracene acts as an energy transfer bridge between Ru^{II*} and Os^{II} creating the basis for an energy transfer "cascade" mechanism and a "molecular light pipe" effect that leads to long range energy transfer [102].

4.3. Amide links to 1:1 poly-styrene–p-aminomethylstyrene

Use of the ether-linked polymers as scaffolds for the study of photochemical electron and energy transfer was limited because of their inability to undergo facile intra-strand energy. There was also a need to develop a more flexible approach to the polymer linkage chemistry. The answer to both was found by turning to an amide-based linkage chemistry and exploiting the well-developed coupling chemistry between amines and carboxylic acids.

The key was to convert the 1:1 styrene–*p*-chloromethylstyrene copolymers into an amine derivative. This was achieved by nucleophilic displacement of chloride by the ph-

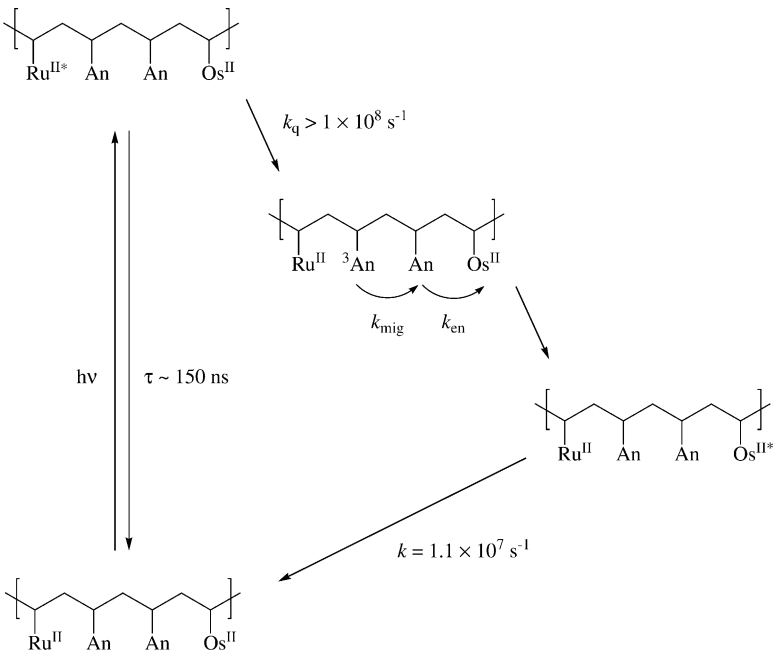

Scheme 9. Intrapolymeric "cascade" energy transfer in 1,2-dichloroethane at 298 K.

thalamide anion in DMF by heating at 100 °C for 8 h. The phthalamide-derivatized polymers were converted to amines by heating in the presence of added hydrazine under reflux in ethanol for 15 h [109].

The acid-derivatized complexes $[M(bpy)_2(bpyCO_2H)]^{2+}$ (M = Ru, Os; $bpyCO_2H$ = 4-methyl-4′-carboxylic acid-2,2′-bipyridine) were added to the polymers by amide coupling in DMF/CH_2Cl_2 solvent mixtures [109].

The linkage reactions are quantitative. Partly loaded polymers were prepared by using the complex as the limiting reagent. The acid–base and redox sensitive amine groups that remained were converted into acetamides by reaction with acetic anhydride in acetonitrile or allowed to react with additional functional groups to prepare multifunctional arrays. The derivatized polymers were purified and characterized by ^{1}H NMR, IR, UV–vis, and electrochemical measurements. A repeat unit of a fully loaded polymer with the appended Ru(II) complex is shown as structure 1 in Fig. 6 [109,110].

Spectroscopic and electrochemical measurements showed that the properties of the polymer-bound complexes were essentially those of isolated monomers. There was evidence for multi-photon effects in fully loaded polymers. Excited state lifetimes became shorter, and highly non-exponential as the irradiance of the incident laser excitation was increased. This was an encouraging observation because it pointed to possible multi-photon excitation followed by rapid intra-strand energy migration. In addition to the multi-photon polarization effects described above, a mechanism for multi-photon quenching exists based on energy migration. If energy migration is rapid on the time scale of the excited state, a mechanism exists for bringing two excited states to adjacent sites where excited state-excited state "annihilation" could occur. There are two reasonable mechanisms for annihilation: (1) sensitization of a higher excited state in one of the partners by the other and (2) excited state-excited state electron transfer which leads to disproportionation and is favored by 1.6 eV [111].

$$-Ru^{II*} - Ru^{II} - Ru^{II*} - \rightarrow -Ru^{II} - Ru^{II*} - Ru^{II*} - \rightarrow -Ru^{II} - Ru^{III} - Ru^{I} - \quad (9)$$

Intra-strand energy migration was investigated in the fully loaded polymer [co-PS-CH_2NHCO-$(Ru^{II})_{11}(Os^{II})_5$]$(PF_6)_{32}$. Corrected emission maxima for Ru^{II*} and Os^{II*} were observed at 640 and 780 nm in CH_3CN, but the Ru^{II*} emission was significantly quenched compared to Ru^{II*} emission in the Ru(II) homopolymer. Analyses of steady-state and transient emission data showed that excitation at Ru(II) is followed by rapid, efficient $Ru^{II*} \rightarrow Ru^{II}$ energy migration and $Ru^{II*} \rightarrow Os^{II}$ energy transfer. The overall efficiency of $Ru^{II*} \rightarrow Os^{II}$ energy transfer following excitation at Ru(II) in CH_3CN at 298 K is >0.9 [110,112].

Based on these results, there is a dramatic difference between the ether and amide linked-polymers in their abilities to enable intra-strand energy transfer. This is true even though both have a three-atom link to the polymer as can be seen by comparing structures (1) and (3) in Fig. 6.

An explanation for the difference has come from transient resonance Raman (TR^3) and transient infrared (TRIR) measurements. Following 368.9 nm excitation and Raman scattering in $[Ru(bpy)_2(bpy)CH_2OCH_2Ph]^{2+}$ ($bpyCH_2OCH_2Ph$ is 4-CH_2Obz-4′-Me-2,2′-bipyridine), which is a model for the ether-linked chromophore, ν(bpy) bands in the region 1000–1700 cm^{-1} are resonantly enhanced. The pattern of enhancements shows clearly that the excited electron is on a bpy ligand and not on the bpy that is ether-linked to the poly-

mer. This is an expected result since the –CH_3 and –CH_2O– groups are electron donating compared to –H which increases the energy of the lowest π^* acceptor orbital on the ether-linked bpy. With bpy as the acceptor ligand, the MLCT excited state dipole is oriented along a Ru-bpy axis pointing away from the polymer backbone and its ~7 Å nearest neighbors [113].

By contrast, in the amide linked polymer the lowest π^* acceptor level is on the bpy that is amide-linked to the polymer. This was demonstrated in the TR^3 spectrum by the appearance of the characteristic pattern of resonantly enhanced bpy-amide bands [110,113]. This conclusion was reinforced by transient infrared measurements in the ν(CO) region by the significant decrease in ν(CO) band energy for the bpy-amide group consistent with reduction of the bpy that is amide-linked to the polymer [114]. Referring to Fig. 6, this aligns the lowest energy MLCT excited state dipole toward the polymer backbone and nearest neighbors which greatly decreases the distance for energy transfer.

The dynamics of excited state quenching and migration in [co-PS-$CH_2C(O)NH$-$(Ru^{II})_{11}(Os^{II})_5$]$(PF_6)_{32}$ were investigated by time-correlated single photon counting in CH_3CN at room temperature. In these experiments, Ru^{II*} emission decay at λ_{max} = 640 nm and growth and decay of Os(II)* at λ_{max} = 780 nm were monitored. Kinetics were nonexponential at both wavelengths, and multi-exponential analysis gave for the average rate constant for nearest neighbor $Ru^{II*} \rightarrow Os^{II}$ quenching, $\langle k \rangle = 4.2 \times 10^8\ s^{-1}$, and for $Ru^{II*} \rightarrow Ru^{II}$ migration, $\langle k \rangle \sim 5 \times 10^7\ s^{-1}$. The magnitudes of these rate constants explain the efficient Ru^{II*} quenching. Energy migration with $\Delta G^\circ = 0$ is the slow step, but it is still 50 times more rapid than Ru^{II*} excited state decay ($k = 1.1 \times 10^6\ s^{-1}$) [115].

Given the complexity of the polymers, the rate constants obtained from the kinetic analysis are the averages of distributions of rate constants. As shown in Scheme 8, energy migration and transfer are kinetically complex. Scheme 8 illustrates the dynamical processes that occur following Ru(II) excitation at sites adjacent, once-removed, and twice removed from an Os(II) quencher. Energy migration is reversible and non-directional which introduces a random walk character to the dynamics. In addition, (1) the polymer samples are distributions of individual strands having varying chain lengths. Individual strands vary in Ru(II)–Os(II) loading pattern which creates a variety of Ru(II)–Os(II) spatial sequences only one of which is illustrated in Scheme 8. (2) The polymer backbones are 1:1 mixtures of styrene and derivatized styrene. Locally, there are regions with no styrene spacer, –M(II)–M(II)–, a single styrene spacer, –M(II)–styr–M(II)–, and two or more spacers, –M(II)–styr–styr–M(II)–. (3) MLCT lifetimes and energy transfer dynamics are dependent on the local environment, and there is a distribution of sites on individual polymer strands [115].

Energy transfer occurs by a through-space mechanism rather than through the 15–20 chemical bonds that, on the average, intervene between Ru^{II*} and Os^{II}. For through-space transfer, local segmental motions could decrease the average periphery-to-periphery distance between nearest neighbors to well below 7 Å.

Even if through-space transfer dominates, the detailed energy-transfer mechanism, whether Förster (coulomb) or Dexter (exchange) or a combination of the two is unknown. Given its $1/R^6$ distance dependence, Förster transfer is favored over Dexter transfer at long distances since Dexter transfer varies exponentially with distance. Förster transfer requires that spin be conserved separately at the energy transfer donor and acceptor. This condition is met even though the Ru(II) and Os(II) ground states are singlets and the excited states nominally "triplets". The lowest energy MLCT "excited states" are actually a manifold of three closely spaced states arising from a lowest energy triplet state split by low symmetry and spin–orbit coupling. Although these states are largely triplet in character, they contain up to ~30% singlet character due to spin–orbit coupling [116].

Procedures are available for fitting Ru^{II*} and Os^{II*} emission spectra to evaluate the kinetic parameters that determine the barrier to energy transfer [117–120]. In the average mode approximation, the parameters are the solvent reorganization energy including low frequency modes treated classically (λ'_{DA}), ΔG°, the quantum spacing ($h\nu = \bar{h}\omega$), and the electron-vibrational coupling constant S. S is related to the change in equilibrium displacement in the averaged coupled vibration by $S = (M\omega\bar{h})(\Delta Q_{eq})^2$ with M the reduced mass. These parameters can be used to calculate the vibrational overlap factor, F_{calc} in Eq. (10) below, and from it and the experimentally measured rate constant, an average energy transfer coupling matrix element, $\langle V_{en} \rangle$. This analysis gave $\langle V_{en} \rangle \sim 2\ cm^{-1}$ for $Ru^{II*} \rightarrow Os^{II}$ energy transfer in [co-PS-$CH_2C(O)NH$-$(Ru^{II})_{11}(Os^{II})_5$]$(PF_6)_{32}$.

$$k_{en} = \left(\frac{2\pi V_{en}^2}{\bar{h}}\right) F_{calc} \tag{10}$$

The results of these experiments demonstrated that the 1:1 styrene polymers with amide linking could support long-range energy transfer. Excited states associated with the polystyrene backbone are too high in energy to be directly involved in the energy transport process. These states and low lying excited states in the solvent contribute indirectly to $\langle V_{en} \rangle$ by mixing with the MLCT excited states [121]. The energy transfer mechanism is by site-to-site, through-space energy transfer hopping. With the excited state dipoles directed toward nearest neighbors, the energy transfer donor–acceptor distances are sufficiently short that facile energy transfer occurs, perhaps by a combination of electronic (Dexter) or through-space (Förster) coupling.

These experiments demonstrated that derivatized polystyrene assemblies could act as relatively efficient "antennae" for harvesting visible light. Light absorption and relaxation convert the initial excitation energy into molecular excited state energy. It is subsequently transferred along the polymer chain by site-to-site energy hopping.

In the natural photosynthetic apparatus, a series of integrated reactions occur in one spatially integrated assembly. The sequential order in Photosystem II is: (1) light is absorbed in an antenna array, (2) energy is transferred from the antenna and sensitizes the excited state of the "special pair" in the reaction center, (3) the special pair excited state undergoes oxidative quenching, (4) spatially directed electron transfer occurs away from the reaction center driven by a free energy gradient, and (5) the oxidized special pair is reduced with transfer of the hole to a manganese cluster where water oxidation occurs.

A derivatized polystyrene assembly has been used to mimic the antenna-sensitization-electron transfer sequence of photosynthesis. In this experiment, the Os(II) quencher site in the mixed Ru(II)–Os(II) amide-linked polymers was replaced by a derivative of the chromophore-donor–acceptor complex in Fig. 5. In this derivative, the bpy ligand was replaced by 4-Me-4′-CO_2H-2,2′-bpyridine to give [Ru(bpy-PTZ)(bpy-MV^{2+})(bpy-CO_2H)]$^{4+}$ (RC for reaction center model) which was attached to the polymer by amide coupling. The antenna-chromophore-electron transfer array [co-PS-CH_2C(O)NH-$(Ru^{II})_{17}(RC)_3](PF_6)_{46}$ was prepared by attaching [Ru(bpy)$_2$(bpyCO_2H)]$^{2+}$ to the remaining amino groups also by amide coupling [122].

Following MLCT excitation by visible laser flash photolysis in CH_3CN at 25 °C, the polymer-bound $PTZ^{\bullet+}$–$MV^{\bullet+}$ redox-separated (RS) state in Scheme 10 was formed as shown by transient absorption measurements. Emission at the chromophore-antenna sites was quenched by ∼34% compared to the $-(Ru^{II})_{20}-$ homopolymer consistent with significant intramolecular quenching. Energy transfer from antenna Ru^{II*} sites to RC sites was favored by −0.1 eV. Based on transient absorption measurements, ∼50% of the RS state was formed during the ∼7 ns laser pulse consistent with significant intra-strand sensitization. The RS state appears by a combination of direct excitation followed by electron transfer at the RC as in Fig. 5 and by indirect sensitization by Ru^{II*} → RC energy transfer followed by electron transfer in the MLCT excited state of the RC complex. There is a significant contribution from excitation at antenna sites not adjacent to RC followed by migration and sensitization [122].

In the overall reaction, the 2.13 eV excited state energy of the antenna-excited states is transferred to the reaction center model where it is converted into 1.15 eV of stored redox energy as a RS state. The efficiency of formation of the RS state varies from 12 to 18% depending on the laser irradiance. At high irradiances, multi-photon excitation and excited state-excited state annihilation compete with sensitized electron transfer [122].

The transient absorption measurements revealed an additional long-lived transient which decayed by second-order, equal concentration kinetics with $k \sim 48\,M^{-1}\,s^{-1}$. It was formed in low efficiency (∼0.5%) and attributed to polymers in which $PTZ^{\bullet+}$ and $MV^{\bullet+}$ were formed on spatially separated RC sites. This result can be explained by invoking mechanisms in which electron transfer quenching of Ru^{II*} by PTZ or MV^{2+} occurs followed by intra-strand hole or electron transfer hopping to a second RC site.

Slow intra-strand $MV^{\bullet+}$ → $PTZ^{\bullet+}$ back electron transfer ($k < 15\,s^{-1}$) is potentially an important observation. It shows that photochemically generated redox equivalents can be created and stored on the polymers for extended periods.

4.4. Amide links to poly-p-aminostyrene

The amino-derivatized version of the 1:1 styrene–chloromethylstyrene polymer provided a versatile synthetic platform for the preparation of multifunctional molecular assemblies with facile intra-strand energy transfer. However, the free radical polymerization method used to make it gives broad molecular weight distributions and high polydispersities. There is also an uncontrollable local structural irregularity arising from random placement of the inert styryl spacers along the polymer backbone.

With these limitations in mind, we investigated a second approach to the preparation of amino-derivatized polymers. It was based on an earlier procedure developed by Nakahama and Hirao [123] involving living anionic polymerization of an amino styryl monomer which gives a product without intervening spacers, Eq. (11). It utilizes a silyl-protected aminoethyl styrene derivative and *sec*-BuLi as the initiator. The chain length of the product is controllable by controlling the ratio of vinyl monomer to initiator. Polymerization was quenched by the addition of methanol and the amino groups deprotected by sequential treatment with strong acid and base. Samples prepared in this way had polydispersities in the range M_w/M_n = 1.10–1.18 [130,131].

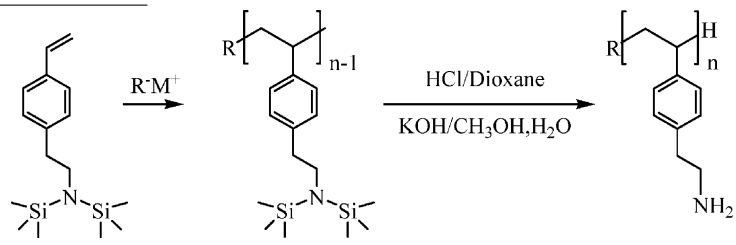

(11)

The polymers were derivatized by amide coupling to the carboxylic acid complexes as described above by using standard amide coupling conditions. Partial loading was achieved by using the complexes as limiting reagents. Unreacted amine sites were used to link additional functional groups or capped with acetamide protecting groups by reaction with acetic anhydride. The contents of the final poly-

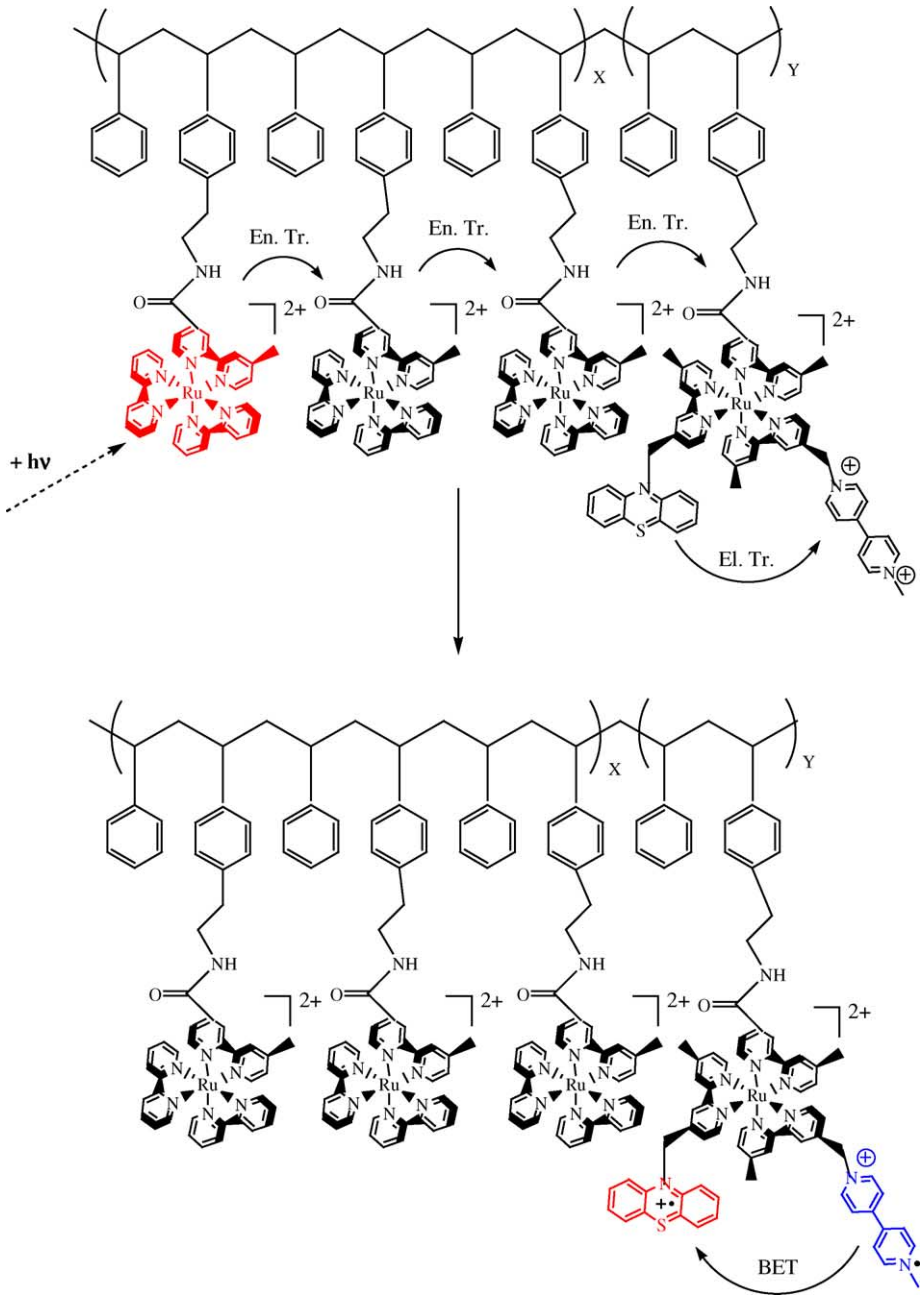

Scheme 10. Indirect sensitization of electron transfer in the polystyrene-based antenna-reaction center model.

mer samples were determined by quantitative ^{1}H NMR integrations.

The structure of a repeat unit of a polymer derivatized by addition of $[Ru(bpy)_2(bpy\text{-}CO_2H)]^{2+}$ is shown as structure 2 in Fig. 6. Compared to the ether-linked and earlier amide-linked copolymers, an additional $-CH_2-$ spacer is inserted in the link to the backbone, and there is no intermediate styryl spacer. The added methylene spacer was a deliberate design feature. It was added to compensate for the loss of the styryl spacers by increasing flexibility and decreasing repulsion between adjacent complexes on the polymer backbone.

A structure of $[PS\text{-}CH_2CH_2C(O)NH\text{-}(Ru^{II})_{20}](PF_6)_{40}$ calculated by a Monte Carlo simulation is shown in Fig. 9 [126]. The large spheres in the structure are the 14 Å cations, and the small spheres are the PF_6^- anions. The calculations reveal that the large excluded volumes of the complexes force the polymers to adopt extended, rod like structures. A metal–metal pair distribution function calculated from the Monte Carlo simulations reveals that each complex in the structure has between four and five nearest neighbors. In more than half of the partially nearest neighbor pairs, the periphery-to-periphery distance is <2 Å. The average distance between peripheries is 2–3 Å.

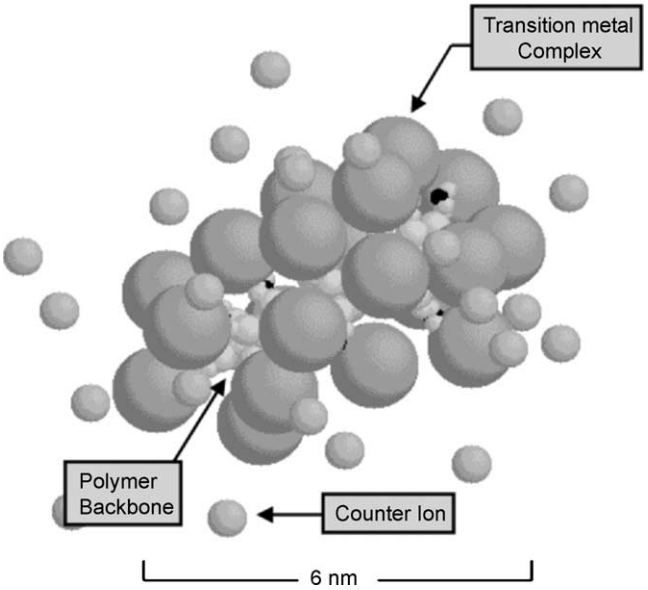

Fig. 9. Molecular structure of $[PS\text{-}CH_2CH_2C(O)NH\text{-}(Ru^{II})_{20}](PF_6)_{40}$ from a Monte Carlo simulation, see text.

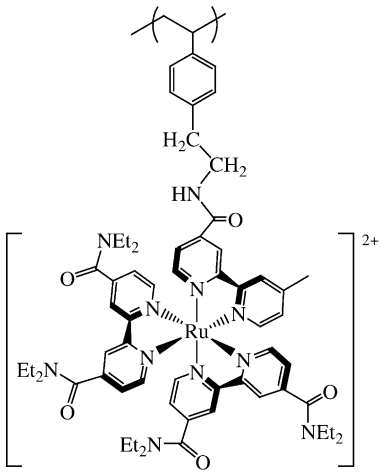

Fig. 11. Structure of the bis-diethylamide derivatized repeat unit.

The spectroscopic and electrochemical properties of the amide-linked complexes are essentially those of the related model complex $[Ru(bpy)_2(bpy)\text{-}C(O)NHCH_2CH_2\text{-}p\text{-}C_6H_4Et]^{2+}$ and the amide-linked complexes in the styrene-based copolymers. There was evidence for multi-photon effects in irradiance-dependent lifetimes attributed to possible excited state-excited state annihilation and local polarization effects [124,125].

A procedure was developed for derivatizing the terminii of the polymer. The chlorosilane derivative $ClSi(CH_3)_2(CH_2)_4N(SiMe_3)_2$ was added to living polymer mixture in Eq. (11) to terminate the polymerization process. Subsequent deprotection of the silyl-protected amine group by sequential acid–base treatment and amide coupling with $[Ru(bpy)_2(bpy\text{-}CO_2H)]^{2+}$ gave the series of polymers shown below with n = 20, 100, and 200. Not unexpectedly, the photophysical properties of the MLCT excited states were the same within experimental error with τ = 1.3 μs (k = 6.0 × $10^5\ s^{-1}$) and emission quantum yields = 0.10 (Fig. 10) [127].

The dynamics of intra-strand energy transfer were investigated in $[PS\text{-}CH_2CH_2C(O)NH\text{-}(Ru^{II}')_{17}(Os^{II})_3](PF_6)_{40}$. In this polymer, the amide link to the polymer backbone was retained, but the remaining two bpy ligands were replaced by 4,4′-bis-diethylamide-substituted (Fig. 11) bpy. The structure of the "antenna" repeat unit is shown below. A population analysis revealed that statistically 24% of the polymer strands have three Os(II) trap sites, 35% have more than three, and 41% have fewer than three [126].

The MLCT excited state energy of this complex is the same as for the bis–bpy complex with λ_{max} = 640 nm. However, the lowest lying π^* levels are on the bis-amide bpy ligands because of the two electron withdrawing amide substituents. This ligand has been shown to be the acceptor in model complexes based on TRIR measurements in the ν(CO) region [128,129]. From the repeat unit structure shown above, this places the lowest MLCT excited state dipole aligned along Ru-bpy$(C(O)NEt_2)_2$ axes pointing away from the polymer backbone. However, the nearest neighbor periphery-to-periphery distance is only 2–3 Å compared to 7 Å in the copolymers.

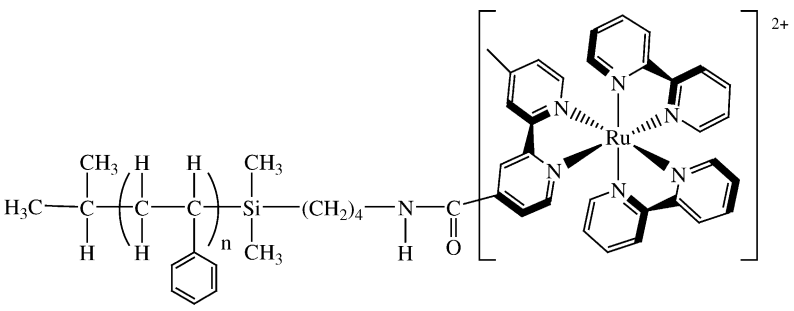

Fig. 10. Structure of terminal N-derivatized polystyrene.

Analysis of steady-state emission and lifetime data revealed that quenching of Ru^{II*} in the mixed polymer was nearly quantitative. Most of the Ru^{II*} emission that was observed came from Ru(II) homopolymer lacking an Os(II) trap site. Interpretation of time-resolved Ru^{II*} corrected emission data at 640 nm and Os^{II*} data at 780 nm by Monte Carlo simulation gave $k = 2.5 \times 10^9\ s^{-1}$ as the most probable $Ru^{II*} \rightarrow Os^{II}$ energy transfer rate constant. The time scale for $Ru^{II*} \rightarrow Ru^{II}$ migration was 1–4 ns ($k = 2.5 \times 10^8\ s^{-1}$ to $1 \times 10^9\ s^{-1}$). Over 80% of the energy transfer, quenching events utilized one or more $Ru^{II*} \rightarrow Ru^{II}$ migration steps. There are contributions to energy transfer from pathways in which there are 100 and more migration steps [126].

Comparison with results on energy transfer in structurally related Ru(II)–Os(II) ligand bridged complexes pointed to energy transfer dominated by a through-space mechanism possibly with contributions from both Förster and Dexter transfer. These results show that the 2–3 Å periphery-to-periphery distance between nearest neighbors is sufficient to promote facile energy migration even with the excited state dipoles aligned away from the polymer backbone. There are contributions to electronic coupling from super-exchange mixing of low-lying polymer and solvent excited states with the MLCT excited states [121,126].

4.5. Photophysical and electron transfer properties in rigid media

The experimental results discussed here on intra-strand polymer dynamics were all obtained in solution. Of greater interest in possible device, applications is the demonstration of photo-induced electron and energy transfer in the rigid environments of composite materials or films, or on surfaces.

The polymer $[PS\text{-}CH_2CH_2NHC(O)\text{-}(Ru^{II})_{18}](Cl)_{36}$ was incorporated into SiO_2 sol–gels by adding the polymer as a component to solutions in which the gel was formed by acid hydrolysis of $Si(OMe)_4$ with Triton-X 100 added as a stabilizer. Stable films of the resulting polymer-gel composites were formed on glass surfaces and on the surfaces of optically transparent, Sn(IV)-doped In_2O_3 (ITO) electrodes for combined spectral-electrochemical measurements. The stability of the resulting gel-polymer film composites toward leaching of the polymer and the spectroscopic, excited state, and oxidation–reduction properties of the polymer in the films were all investigated [130,131].

The polymer-containing thin film composites are open to small molecule diffusion from the external solution. Based on cyclic voltammetry measurements on the Ru(III)/(II) couple in the films, the Ru(II) polymers can act as redox mediators toward the Os(II) polymer $[PS\text{-}CH_2CH_2CNHC(O)(Os^{II})_{20}](PF_6)_{40}$ in an external solution since the polymer is too large to diffuse through the films [131]. Ru^{II*} excited state decay is multi-exponential and kinetically complex as expected. There is a distribution of emitting sites and multi-photon effects arising from excited state-excited state interactions decrease lifetimes and introduce light intensity effects [130].

Electrogenerated chemiluminescence (ecl) was observed from the films by cycling the potential of the underlying electrode past the potential for the Ru(III/II) couple in the presence of oxalate anion in the external solution [130]. Ru(III) is generated during oxidative scans, and one-electron oxidation of oxalate anion, $C_2O_4^{2-}$, gives the radical $C_2O_4^{-}$. It is a sufficiently strong reductant that it undergoes electron transfer to Ru(III) to give the excited state, $Ru^{III} + (C_2O_4)^- \rightarrow Ru^{II*} + 2\ CO_2$. A related chemistry between $C_2O_4^{2-}$ and $[Ru(bpy)_3]^{3+}$ in solution has been described by Bard and coworkers [132].

Electro-luminescence was also observed by cycling the underlying electrode over a potential range sufficient for oxidation of Ru(II) to Ru(III) followed by reduction of Ru(II) to Ru(I) ($Ru^{II}(bpy^{\bullet -})$). Emission is induced within the films by electron transfer from Ru(I) to Ru(III) to give Ru^{II*} by the reaction, $Ru^{I} + Ru^{III} \rightarrow Ru^{II} + Ru^{II*}$, which is favored by $\Delta G^\circ = -0.6$ eV [130].

Intra-strand $Ru^{II*} \rightarrow Os^{II}$ energy transfer was investigated in $[PS\text{-}CH_2CH_2C(O)NH\text{-}(Ru^{II'})_{17}(Os^{II})_3](PF_6)_{40}$ containing the Ru^{II} amidebpy complex in Figure 11 in frozen 5:4 (v:v) butyronitrile:propionitrile solutions at 77 K, in polymethyl (methacrylate) (PMMA) films, and in SiO_2 xerogel monoliths. Comparisons of steady-state emission spectra for the mixed polymer and the homopolymer $[PS\text{-}CH_2CH_2C(O)NH\text{-}(Ru^{II'})_{20}](PF_6)_{40}$ in solution and in the three rigid media reveal that extensive $Ru^{II*} \rightarrow Os^{II}$ energy transfer continues to occur in all three rigid media. The extent of quenching is medium dependent decreasing in the order: PMMA > SiO_2 xerogel > 77 K nitrile glass [133]. Transient emission monitoring by time-correlated single photon counting at 640 nm for Ru^{II*} and at 730 nm for Os^{II*} reveals that the majority of the Ru^{II*} decay, which occurs on the ∼ns time scale, coincides with a growth in Os^{II*} emission. The dynamical observations are consistent with rapid, efficient $Ru^{II*} \rightarrow Os^{II}$ energy transfer.

Continued energy transfer and migration in rigid media was explained by applying energy transfer theory. The classical barrier to energy transfer is actually decreased in a rigid medium compared to a comparable fluid. This is because the orientational polarization is frozen. In solution, this polarization reorients to the charge distribution of the excited state. Solvent reorientation at both the excited state donor and ground state acceptor contribute to the energy transfer barrier. A related analysis has been applied to excited state electron transfer in rigid media where medium and counter ion effects play a more important role [134].

Time-resolved emission decay dynamics for $[PS\text{-}CH_2CH_2C(O)NH\text{-}(Ru^{II})_{17}(Os^{II})_3](PF_6)_{40}$, the two homopolymers $[PS\text{-}CH_2CH_2C(O)NH\text{-}(M^{II})_{20}](PF_6)_{40}$ (M^{II} = Ru^{II} and Os^{II}), and the model complexes $[M(bpy)_2(4,4'\text{-}(C(O)NEt_2)_2\text{-}bpy)]^{2+}$ (M = Ru and Os) were analyzed in PMMA [135]. Direct evidence for facile $Ru^{II*} \rightarrow Ru^{II}$ migration and $Ru^{II*} \rightarrow Os^{II}$ energy transfer was obtained by

time-correlated single photon counting in the frozen nitrile mixture. Non-exponential decay kinetics and red-shifted, time-dependent emission spectra were observed even for the homopolymers. These effects were attributed to local inhomogeneities and rigidity which create a distribution of sites. Excitation is followed by excited state migration to low energy sites which causes a time-dependent red shift in the emission and decreased lifetimes. Emission lifetimes are decreased because of the smaller excited-to-ground state energy gaps at the lower energy sites. Related phenomena appear for organic excited states in rigid media [136] and MLCT excited states in electropolymerized films [137].

5. Oligoproline assemblies

The experiments with polystyrene demonstrated the viability of derivatized polystyrene as a scaffold for constructing multifunctional molecular assemblies. With the amide linkage chemistry and anionic polymerization, polymer samples can be prepared having variable and relatively narrow molecular weight distributions. In these polymers, the relatively large Ru(II) and Os(II) polypyridyl complexes enforce rod-like structures with closely spaced nearest neighbors. Intrastrand energy migration is rapid. Energy transfer continues to occur in rigid media. The results with the antenna-reaction center model polymer show that the polystyrene scaffold can support and promote multiple functions in the same molecular array.

The use of pre-formed polymers has the significant disadvantage that there is no control over the relative spatial disposition of functional groups as they are added to the polymer. Even in a partly loaded homo-polymer, with a single type of added functional group, the spatial loading along the polymer backbone is presumably random perhaps oriented somewhat by the molecular volumes of the groups added and electrostatic effects.

We turned to solid phase peptide synthesis and the step-by-step construction of oligopeptides as a way to control the spatial dispositions of added functional groups [138]. The goal was to prepare chromophore-electron transfer assemblies with control of both spatial disposition of added groups and the three-dimensional structure of the resulting assembly.

5.1. Amino acid assemblies

An initial assembly was prepared based on triple derivatization of the amino acid lysine (Lys- $H_2NCH_2(CH_2)_4NH_2)CO_2H$ which contains an amino group in a side chain of the amino acid. $[Ru(bpy)_2(bpy\text{-}CO_2H)]^{2+}$ was first coupled with the BOC-protected amino acid (BOC is 1,1-dimethylethyloxycarbonyl), and the electron transfer acceptor and donor were subsequently added in sequential steps. In the amide coupling reactions, *N*,*N*′-dicyclohexylcarbodiimide was added as a dehydrating agent, *N*-methylmorpholine as a base, and 4-(dimethylamino)pyridine as an acylation catalyst [138–140].

As illustrated in Scheme 11, MLCT excitation of the resulting assembly in CH_3CN at 298 K is followed by electron transfer quenching of the MLCT excited state, presumably by initial oxidative electron transfer to MV^{2+} and rapid PTZ $\rightarrow$ Ru^{III} electron transfer, to give the PTZ^{+}–MV^{+}-based, 1.14 eV redox-separated state. The RS state is formed with an efficiency of 0.34 and undergoes back electron transfer with $k = 6.8 \times 10^6\ s^{-1}$ [141–143].

5.2. Oligoproline assemblies by solid-state peptide synthesis

Preparation of the lysine-based donor-chromophore–acceptor complex (Scheme 11) demonstrated the feasibility of preparing complex redox assemblies by high yield amide coupling reactions. The next step in preparing large-scale

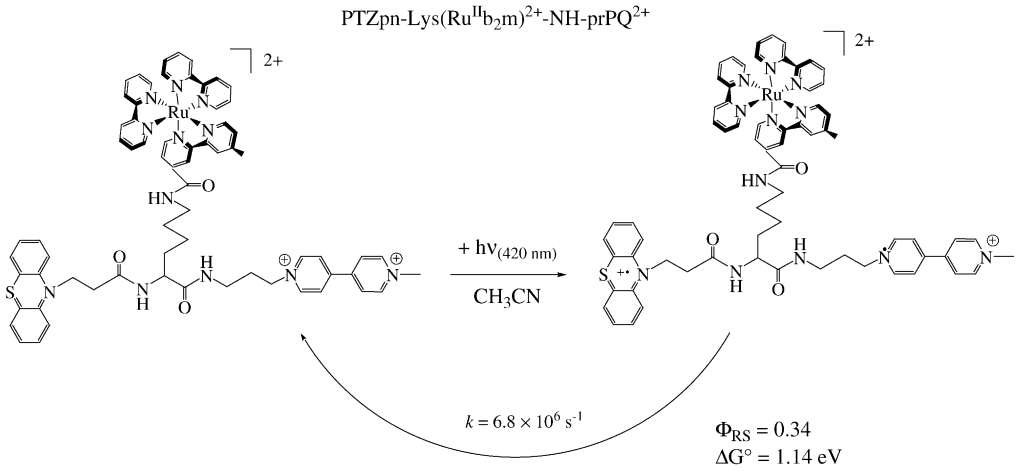

Scheme 11. Photochemical electron transfer scheme.

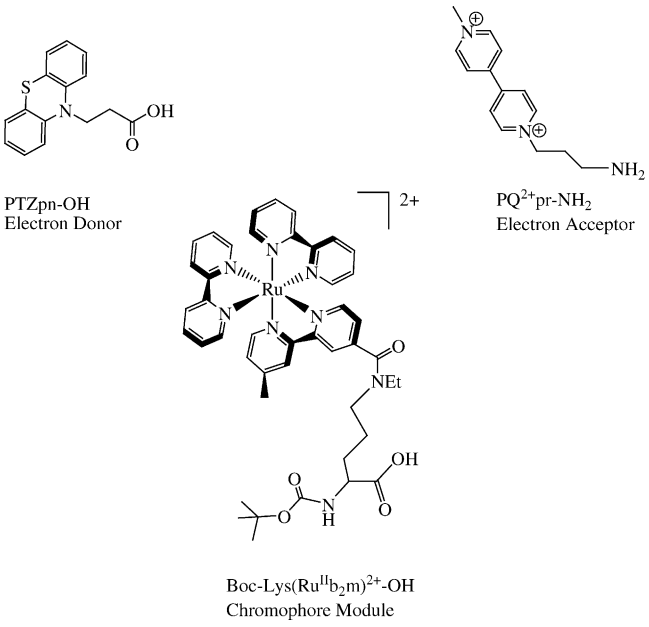

Fig. 12. Components of the lysine-based donor-chromophore–acceptor assembly.

assemblies was to exploit solid-state peptide synthesis. This was a technique pioneered by Merrifield and coworkers in which oligopeptides are prepared on a solid support by stepwise amide coupling [144].

A BOC-protected amino acid is first bound to a solid support, typically a chemically derivatized resin containing an amine, for example, a methylbenzhydrylamine-resin. Deprotection of the Boc protecting group frees the amine group for amide coupling. As shown in Eq. (12) with P the solid support, subsequent amide coupling with a second Boc-protected amino acid or oligopeptide adds to the growing oligopeptide on the resin. The stepwise nature of the procedure provides control over the order of addition and thus the spatial composition of the oligopeptide. In the final step, the peptide assembly is cleaved from the solid support.

$$\text{P-C(O)C(R)NH-Boc} \xrightarrow{\text{-Boc}} \text{P-C(R)NH}_2$$
$$\xrightarrow{+\text{Boc-NHC(R}'\text{)CO}_2\text{H}} \text{P-C(O)C(R)NHC(O)C(R}'\text{)NH-Boc} \quad (12)$$

Gaining control of the three-dimensional structure of the resulting assemblies required an additional feature. Proline is the only natural cyclic amino acid. An oligoproline chain of nine or more prolines folds into a stable helix even with relatively large functional groups on the proline side chains. As shown in Fig. 13, there are two helical forms of polyproline, Pro I and Pro II. Pro I is a right-handed helix consisting locally of *cis*-amide bonds and is favored in non-polar solvents. The structure repeats itself every 3.3 residues with a repeat spacing along the helix of 6.6 Å. Pro II is a left-handed helix with local *cis*-amide bonds, repeats itself with three residues per turn, has a repeat spacing of 9.4 Å, and is favored in polar solvents, notably water. Polyproline spacers had been used previously to study distance effects in intramolecular electron transfer [145–148].

Exploiting the oligoproline helical structural motif as a scaffold for photochemical assemblies required preparation of appropriate synthetic amino acids containing a chromophore and electron transfer donors and acceptors combined with solid-state peptide synthesis. This was accomplished by first preparing the L optical isomer of the azidoproline shown as **2** in Scheme 12 and reducing it to the amine. The amine group was Boc-protected and then amide coupled with $[Ru(bpy)_2(bpy\text{-}CO_2H)]^{2+}$ and carboxylic acid derivatives of PTZ and the electron transfer acceptor anthraquinone.

With the series of Boc-protected amino acids in hand, solid-state peptide synthesis was used to construct the 13-residue oligoproline shown in Fig. 14. The line structure in Fig. 14 clearly illustrates the relative positions of the functional groups. The use of two proline spacers between func-

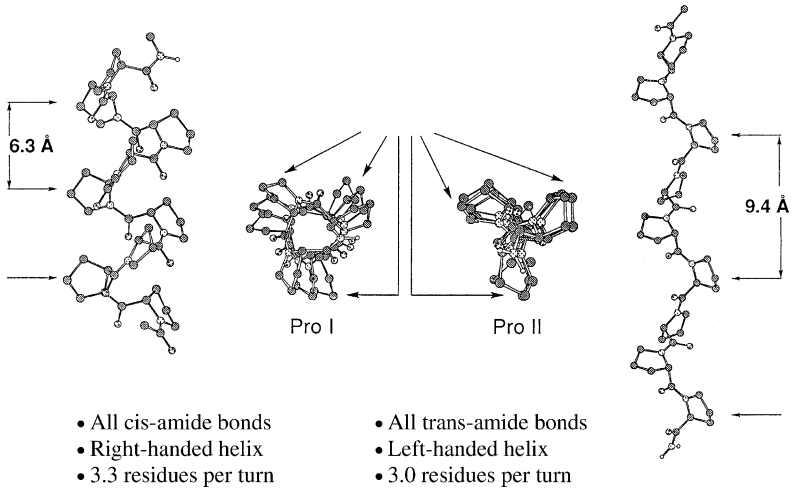

Fig. 13. Structural details of Pro I and Pro II oligoproline helices.

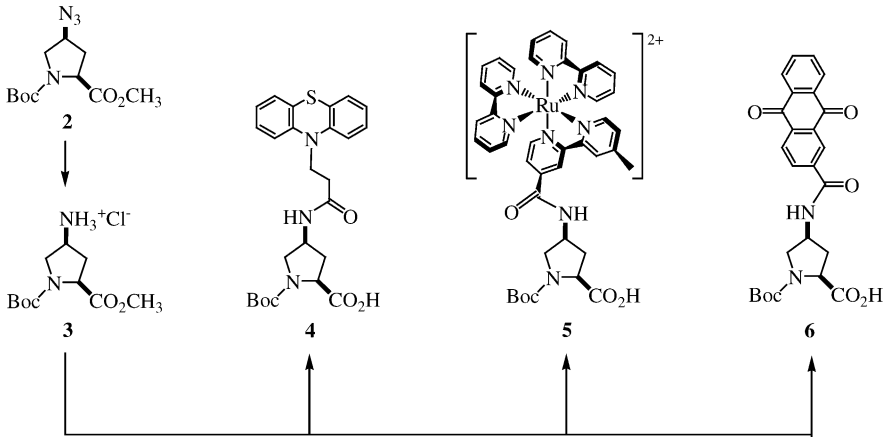

Scheme 12. Synthesis of Boc-protected proline redox modules.

tional groups favors the Pro II helix over Pro I because the larger helical repeat distance for Pro II decreases steric repulsion. The terminal CH_3CO-Pro_3- and -Pro_3-NH_2 segments allow the helix to begin and end with a capped Pro_3 turn which helps to prevent unwinding of the helix.

Circular dichroism (CD) measurements in the $n \rightarrow \pi^*$, $\pi \rightarrow \pi^*$ amide region in the UV show that the 13-residue oligoproline adopts the Pro II helical structure in water. It is a stable structure, heating to 85 °C resulted in minimal change in the CD spectrum [149]. The structure is maintained in CH_3CN even though non-polar solvents typically favor Pro I. As noted above, this is a consequence of the -Pro_2- spacers and the large appended functional groups which favors the more open Pro II helix.

The same assembly, but with Pro_7 termini, does undergo Pro II and Pro I interconversion in CH_3CN, at least at the Pro_7 termini. The kinetics are complex but could be fit to a bi-exponential kinetic expression with $k_1 = 3.3 \times 10^{-4}\ s^{-1}$ and $k_2 = 0.8 \times 10^{-4}\ s^{-1}$ consistent with an unwinding-rewinding process involving a series of intermediates [150].

The space filling structure in Fig. 14 was calculated by using Biosym Insight II (Biosym Technologies). It illustrates the three-dimensional spatial extension of the oligopeptide assembly and the lining up of the appended functional groups along the oligproline backbone in the Pro II helix. The structure also illustrates the electron transfer events that are triggered following MLCT excitation at 460 nm.

The dynamic electron transfer properties of the assembly following MLCT excitation were investigated by ns transient absorption and emission measurements in CH_3CN at 298 K. MLCT excited state quenching and the appearance of $PTZ^{\bullet+}$ (λ_{max} = 510 nm) and the anthraquinone radical anion ($Anq^{\bullet-}$, λ_{max} = 590 nm) occurred simultaneously on a time scale of 20 ns to give the final

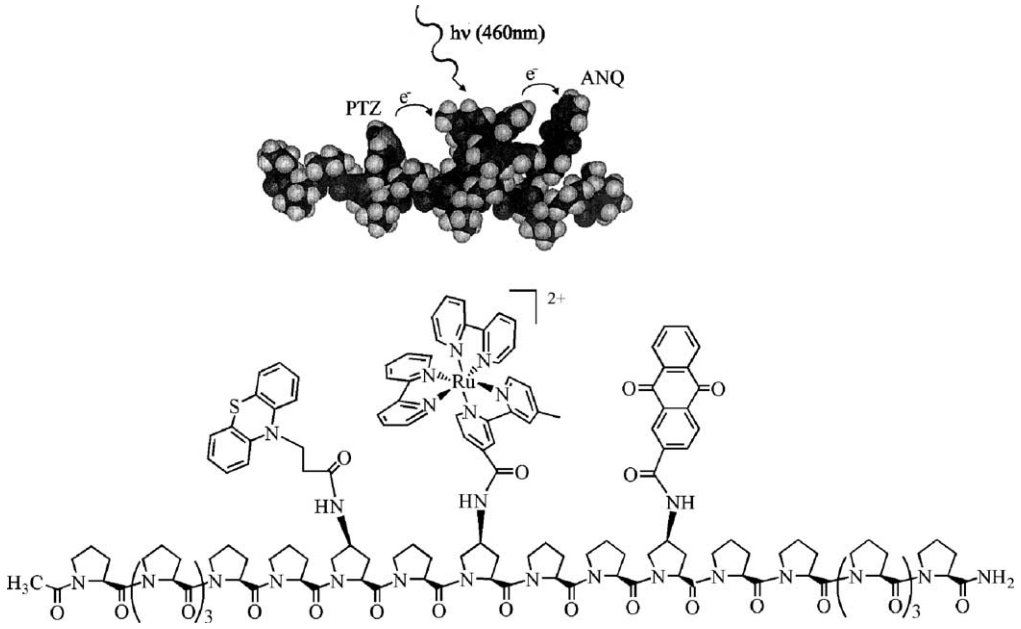

Fig. 14. Two views of oligoproline assembly (**1**).

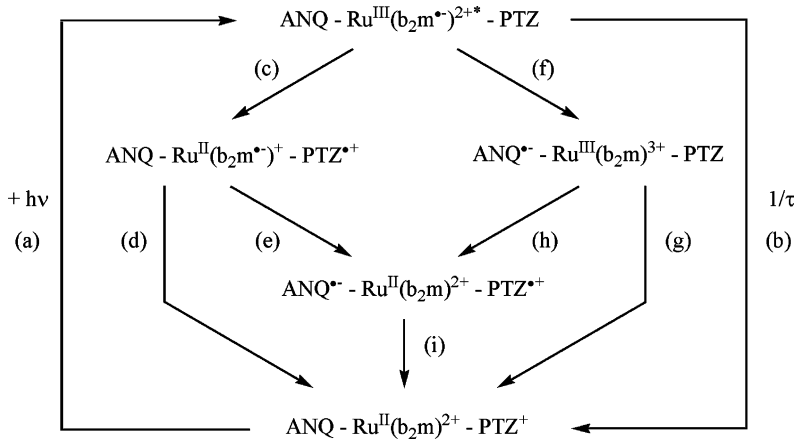

Scheme 13. Kinetic scheme following MLCT excitation of oligoproline assembly (**1**).

redox-separated state CH_3CO-pro_3-pra([$PTZ^{\bullet+}$]pn)-Pro_3-pra($Rub_2m)^{2+}$-Pro_2-pra($Anq^{\bullet-}$)-Pro_3NH_2. The RS state was formed in 53% efficiency, stored 1.65 eV relative to the ground state, and returned to the ground state by $Anq^{\bullet-} \rightarrow PTZ^{\bullet+}$ electron transfer with $k = 5.7 \times 10^6\ s^{-1}$ [149,151].

The effect of solvent on the appearance and decay of the redox-separated state by the reactions in Scheme 13 was investigated in solvents ranging from dichloroethane to dimethylacetamide. Quenching is dominated by PTZ reductive electron transfer (reaction c in Scheme 13) which is favored by $\Delta G^\circ = -0.24$ to -0.44 eV depending on solvent. Quenching is followed by rapid $m^{\bullet-} \rightarrow$ Anq electron transfer (reaction (e)) which gives the RS state. There is a solvent dependent competition between reaction e and $m^{\bullet-} \rightarrow PTZ^{\bullet+}$ back electron transfer to give the ground state (reaction (d)) with the yield of RS state varying from 33 to 96% depending on solvent [151].

Depending on the solvent, the transient energy stored in the RS state varied from 1.46 to 1.71 eV. The rate constant for $Anq^{\bullet-} \rightarrow PTZ^{\bullet+}$ back electron transfer (reaction (i)) was also solvent dependent with k varying from 5.2×10^6 (dichloroethane) to $7.7 \times 10^6\ s^{-1}$ (butyronitrile) at $22 \pm 2\,^\circ$C. Back electron transfer occurs by direct, probably through-space electron transfer (see below). The indirect pathways involving reversal of the electron transfer chains: (1) $Ru^{II} \rightarrow PTZ^{\bullet+}$ electron transfer to give $Anq^{\bullet-}$–$Ru^{III}(b_2m)^{3+}$–PTZ followed by rapid $Anq^{\bullet-} \rightarrow Ru^{III}$ electron transfer, reaction (g), and (2) $Anq^{\bullet-} \rightarrow$ m electron transfer to give Anq–$Ru^{II}(b_2m^{\bullet-})^{+}$–$PTZ^{\bullet+}$ followed by rapid $m^{\bullet-} \rightarrow PTZ^{\bullet+}$ electron transfer, pathway (d)- can be ruled out on energetic grounds [151].

The electron transfer matrix element, $H_{DA} = 0.13$ eV, was estimated by an independent evaluation of the parameters defining the electron transfer barrier. The magnitude of H_{DA} presumably reflects the extent of coupling between the singlet component of the RS state and the singlet ground state with back electron transfer occurring by spin allowed $^1(PTZ^{\bullet+}$–$Anq^{\bullet-}) \rightarrow {}^3$(PTZ–Anq) electron transfer. The largely triplet spin character of the initial MLCT excited state is expected to be largely retained in the initial electron transfer product, $^3(PTZ^{\bullet+}$–$Anq^{\bullet-})$, but $^3(PTZ^{\bullet+}$–$Anq^{\bullet-}) \leftrightarrow {}^1(PTZ^{\bullet+}$–$Anq^{\bullet-})$ spin interconversion is expected to be rapid with the ^{3}RS and ^{1}RS states nearly degenerate [151]. The dominant mechanisms for $^3RS \rightarrow {}^1$RS spin interconversion are anisotropic hyperfine coupling and electron spin–spin dipolar interactions [152,153].

The solid-state peptide synthesis technique allows variations to be made in the order of groups added, the number of intervening spacers, and the number of pro groups at the termini. We have used this flexibility to prepare a series of oligoproline assemblies with the goals of extending the synthetic chemistry, exploring fundamental issues in photochemical electron and energy transfer, and pursuing possible applications in artificial photosynthesis.

In Fig. 15 are shown line structures for two oligoprolines designed to explore the role of distance on intra-helical electron and energy transfer dynamics. In these assemblies, electron withdrawing 4,4′-pyrrolidine-substituted amide groups were added to the bpy ligands to increase the potential of the MLCT excited state as an oxidant in order to ensure that excited state quenching occurred by PTZ reduction and reaction (c) in Scheme 13. This increases the yield of the $PTZ^{\bullet+}$–$Anq^{\bullet-}$ RS state. The substituent change decreases ΔG° for PTZ $\rightarrow Ru^{II*}$ reductive quenching from -0.1 eV to -0.3 eV and increases ΔG° for Anq oxidative quenching from 0 to +0.1 eV. The Pro_7 terminal segments were added to provide nucleation sites for interconversion between the Pro I and Pro II helices at the termini [154].

Quenching of assembly ZRA2 in CH_3CN at 25 °C was 90% complete and occurred with $k = 2 \times 10^7\ s^{-1}$ to give the RS state CH_3CO-Pro_7-pra($PTZ^{\bullet+}$)-Pro_2-pra($Ru(p)_2m]^{2+}$-pro_2-pra(Anq^{-})-Pro_7-NH_2 as shown by transient absorption measurements. Once formed, the RS state underwent $PTZ^{\bullet+} \rightarrow Anq^{\bullet-}$ back electron transfer to give the ground state with $k_{ET} = 4.8 \times 10^6\ s^{-1}$. This rate constant is the same within experimental error as the rate constant for back electron transfer in assembly **1** (ZRA1) showing that replacement of the pro_3

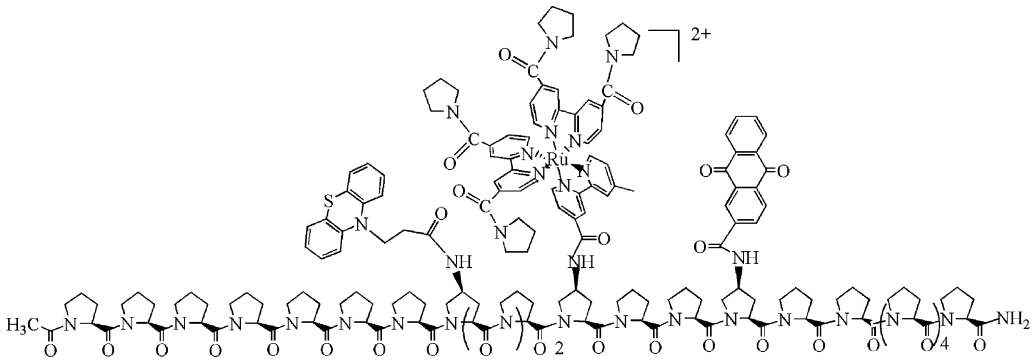

ZRA2, CH_3-CO-Pro_7-Pra(PTZpn)-Pro_2-Pra($Ru^{II}p_2m)^{2+}$-Pro_2-Pra(Anq)-Pro_7-NH_2

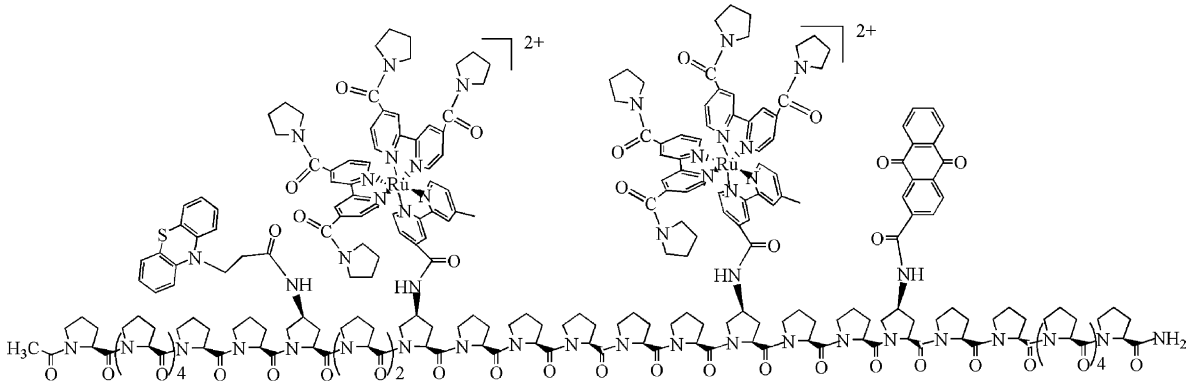

ZRRA, CH_3-CO-Pro_7-Pra(PTZpn)-Pro_5-Pra($Ru^{II}p_2m)^{2+}$-Pro_2-Pra(Anq)-Pro_7-NH_2

Fig. 15. Line structures for the amide-derivatized oligoprolines.

termini by Pro_7 termini has a negligible effect on intra-helical electron transfer dynamics [154].

In assembly ZRRA, 13 proline spacers intervene between PTZ and Anq. The spatial demands on electron transfer in reaching the $PTZ^{\bullet+}$–$Anq^{\bullet-}$ RS state are considerable. Excitation at the Ru(II) complex adjacent to PTZ, Ru(II,a) followed by PTZ → Ru^{II*} quenching would give the $PTZ^{\bullet+}$–Ru(II)$p^{\bullet-}$ electron transfer pair. In order for the $PTZ^{\bullet+}$–$Anq^{\bullet-}$ RS state to be reached that long distance, electron transfer must occur between the reduced bpy-pyrrolidine ligand and Anq by $p^{\bullet-}$ → Anq electron transfer. This could occur by the hopping mechanism in Eq. (13) in which inter-complex $p^{\bullet-}$ → p electron transfer is followed by $p^{\bullet-}$ → $PTZ^{\bullet+}$ electron transfer.

$$\begin{aligned}
&\xrightarrow{+h\nu} \rightarrow -(PTZ^{\bullet+})\text{-}Pro_2\text{-}[Ru^{II}(p^{\bullet-})(p)m]^{+}\text{-}Pro_5\text{-}\\
&[Ru^{II}(p)_2m]^{2+}\text{-}Pro_2\text{-}(Anq)\text{-} \rightarrow (PTZ^{\bullet+})\text{-}Pro_2\text{-}\\
&[Ru^{II}(p)_2m]^{2+}\text{-}Pro_5\text{-}[Ru^{II}(p^{\bullet-})(p)m]^{+}\text{-}Pro_2\text{-}(Anq)\text{-}\\
&\rightarrow (PTZ^{\bullet+})\text{-}Pro_2\text{-}[Ru^{II}(p)_2m]^{2+}\text{-}Pro_5\text{-}[Ru^{II}(p)_2m]^{2+}\text{-}\\
&\text{-}Pro_2\text{-}(Anq^{\bullet-})\text{-} \qquad (13)
\end{aligned}$$

Excitation at the Ru(II) complex adjacent to Anq, Ru(II,b), is unproductive in a direct sense. Oxidative electron transfer quenching by Anq does not occur because the reaction is unfavorable thermodynamically. However, excitation at Ru(II,b) can contribute to the appearance of the RS state by initial Ru(II,b)* → Ru(II,a) energy transfer followed by the electron transfer sequence in Eq. (13). The quenching efficiency for ZRRA in CH_3CN is only 60% suggesting that Ru(II,b)* → Ru(II,a) energy transfer is slow relative to the lifetime of Ru(II,b)*, but that it still contributes since the overall efficiency exceeds 50%. This is consistent with the results of direct measurements described below. In ZRRA, the spatial demands on electron transfer and the fact that quenching is only 60% complete combine to decrease the yield of RS state to 20% of that observed in ZRA2 [154].

Back electron transfer between $Anq^{\bullet-}$ and $PTZ^{\bullet+}$ in ZRA2 is essentially temperature independent. This rules out a mechanism involving reversal of the electron transfer chains, e.g., by $Anq^{\bullet-}$ → $[Ru(p)_2m]^{2+}$ → $PTZ^{\bullet+}$ or $[Ru(p)_2m]^{2+}$ → $PTZ^{\bullet+}$ followed by $Anq^{\bullet-}$ → $[Ru(p)_2m]^{3+}$ electron transfer since ΔG° = +0.19 and +0.63 eV for the initial electron transfer steps. The dominant mechanism is long-range, through-bond or through-space $Anq^{\bullet-}$ → $PTZ^{\bullet+}$ electron transfer. In ZRRA compared to ZRA2, there is an increase in the number of covalent bonds between the electron transfer donor and acceptor from 29 to 47. This causes a decrease in the rate constant for back electron transfer by a factor of ∼10 to $5.0 \times 10^5\ s^{-1}$ [154].

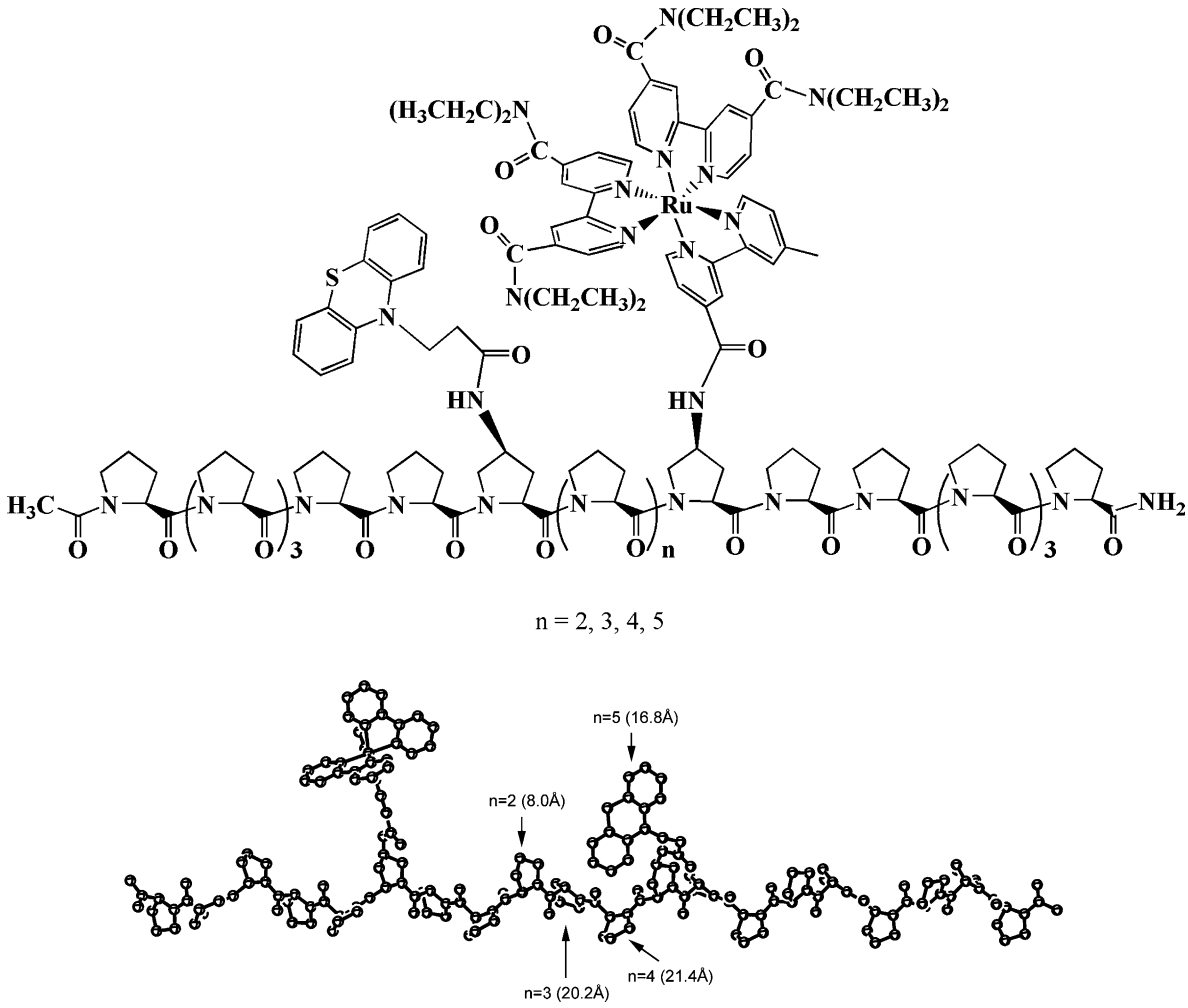

Fig. 16. Line and calculated structures for the Ru(II)-PTZ oligopeptides.

The kinetics of back electron transfer in ZRRA in CH_3CN were studied in both the Pro I and Pro II helical forms. The kinetics of interconversion between the two had been studied earlier by time-dependent CD measurements [150]. For the back electron transfer study, ZRRA was isolated in the Pro II form following aqueous purification by chromatography. The kinetics of back electron transfer in CH_3CN were measured before significant Pro II → Pro I interconversion had occurred (0.5 h). The experiment was repeated after 36 h when conversion was complete. The rate constants for $Anq^{\bullet -}$ → $PTZ^{\bullet +}$ electron transfer in the Pro I and Pro II helices were the same within experimental error, $k = 5 \times 10^5\ s^{-1}$ [154].

This was cited as evidence for a through-bond electron transfer mechanism. There are 47 intervening covalent bonds between $Anq^{\bullet -}$ and $PTZ^{\bullet +}$ in either helix, but the through-space distance is longer by ∼14 Å for Pro II compared to Pro I. However, as noted below, there is relatively clear evidence for through-space electron transfer in a related series of oligoproline assemblies. An alternate explanation is that Pro II → Pro I interconversion only occurs at the pro_7 termini.

An important next step was a systematic investigation of the kinetics of intra-helix electron and energy transfer. The first study investigated the distance dependence of electron transfer in the series of Ru(II)–PTZ assemblies shown in Fig. 16. They were constructed by solid-state peptide synthesis.

Both a line structure and a structure calculated by using the MM4 method implemented in the SPARTAN 5.11 package (Wavefunction Inc.) are shown in Fig. 16. In the actual assembly, the amide-derivatized bpy ligand, 4,4′-(C(ONEt$_2$))bpy, was used in place of bpy to ensure rapid Ru^{II*} excited state quenching by PTZ. A high-level ab initio calculational method based on Density Functional Theory (DFT) was used to calculate the structures of the Ru(bpy)-proline and PTZ-proline residues. In these calculations, the complexes were simplified by using bpy rather than amide-bpy [155]. The DFT calculations revealed that there is a significant H-bonding interaction between the proton on the N atom of PTZ and the CO of an adjacent amide group as shown by the tilt of the PTZ group shown in Fig. 16. The through-space distances from the S atom of the PTZ to the center of the Ru(II) complex

vary from 8.0 to 21.4 Å as the number of intervening prolines (n) is varied from two to five. Through-space distances for $bpy(C(O)NEt_2)^- \rightarrow PTZ^{\bullet+}$ back electron transfer following PTZ → electron transfer quenching vary in the same way, but the distance variation is from 5.0 to 18.4 Å. These are the through-space distances from the S atom of PTZ to the center of the nearest $bpy(C(O)NEt_2)_2$ ligand.

The assemblies exist in the Pro II form in water. Excited state quenching in water occurs in the normal region with $\Delta G^\circ = -0.1$ eV. Quenching is temperature dependent with $E_a \sim 2$ kcal/mol consistent with activated electron transfer. Back electron transfer is highly favored with $\Delta G^\circ = -1.8$ eV and occurs in the inverted region. It is essentially activation-less with $E_a \sim 0$ as expected for electron transfer in the inverted region and excited state nonradiative decay [69,117,156].

The kinetics of Ru^{II*} quenching by PTZ were monitored by transient absorption and emission and $[bpy(C(O)NEt_2)_2]^{\bullet-} \rightarrow PTZ^{\bullet+}$ back electron transfer by transient absorption. The rate constants decrease by $\sim 10^3$ as n was varied from 2 ($k = 2 \times 10^9\ s^{-1}$) to 4 ($2 \times 10^6\ s^{-1}$), but k_{ET} increases by ~10 between $n = 4$ and 5. The increase in the number of proline spacers by one increases the through bond distance, but the through-space distance decreases because of the helical repeat in the oligoproline scaffold, Fig. 16. This observation is inconsistent with simple through-bond electron transfer [155].

The distance dependence of k_{ET} includes contributions from both the electron transfer matrix element (H_{DA}) and the solvent reorganization energy (λ_0). Including both gives the expressions in Eq. (14) for the distance dependences of through-bond or through-space electron transfer in the normal and inverted regions. The terms that appear in Eq. (14) are:

- β: the distance attenuation factor;
- r and r_0: the through-bond distances (4.9 or 3.3 Å per proline; residue) with $r_0 = 5.0$ Å ($n = 2$) as the reference distance;
- d and d_0: the corresponding through-space distances with $d_0 = 8.0$ Å;
- D_{op} and D_s: the optical and static dielectric constants of the medium;
- $\hbar\omega$ and S: the quantum spacing and electron-vibrational coupling constant for the vibrational mode coupled to the transition in the average mode approximation.

$$\gamma = \ln\left(\frac{E_0}{S\hbar\omega}\right) - 1$$

E_0: the energy gap ($=\Delta G^\circ - \lambda_0$)

Through bond:

$$k_{ET} = k_{ET}(r,d) = k_{ET}(r_0,d_0)\ \exp -[\beta(r-r_0)]\ \exp\ \delta \times \left[e^2\left(\frac{1}{d_0}-\frac{1}{d}\right)\left(\frac{1}{D_{op}}-\frac{1}{D_s}\right)\right]$$

$$\delta = \frac{-1}{4RT} \quad \text{(normal region)}$$

$$\delta = \left(\frac{\gamma+1}{\hbar\omega}\right)^2 RT \quad \text{(inverted region)} \tag{14}$$

Through space:

$$k_{ET} = k_{ET}(d) = k_{ET}(d_0)\ \exp -[\beta(d-d_0)]\ \exp\ \delta \times \left[e^2\left(\frac{1}{d_0}-\frac{1}{d}\right)\left(\frac{1}{D_{op}}-\frac{1}{D_s}\right)\right]$$

The experimental rate constants were corrected for the solvent dependence predicted by Eq. (14) by defining $k'_{ET} = k_{ET}\exp-\{\delta[e^2((1/d_0)-(1/d))((1/D_0)-(1/D_s))]\}$. According to Eq. (14), through-bond and through-space electron transfer are predicted to have distinctly different distance dependences in both the normal and inverted regions. $\ln k'_{ET}$ is predicted to vary with $r - r_0$ for through-bond electron transfer and with $d - d_0$ for through-space transfer [155].

It is apparent from the plots of $\ln k'_{ET}$ versus $r - r_0$ and $\ln k'_{ET}$ versus $d - d_0$ in Fig. 17 for electron transfer in the normal region (for the quenching step $k'_{ET} = k'_2$) that the data fit the latter and not the former consistent with

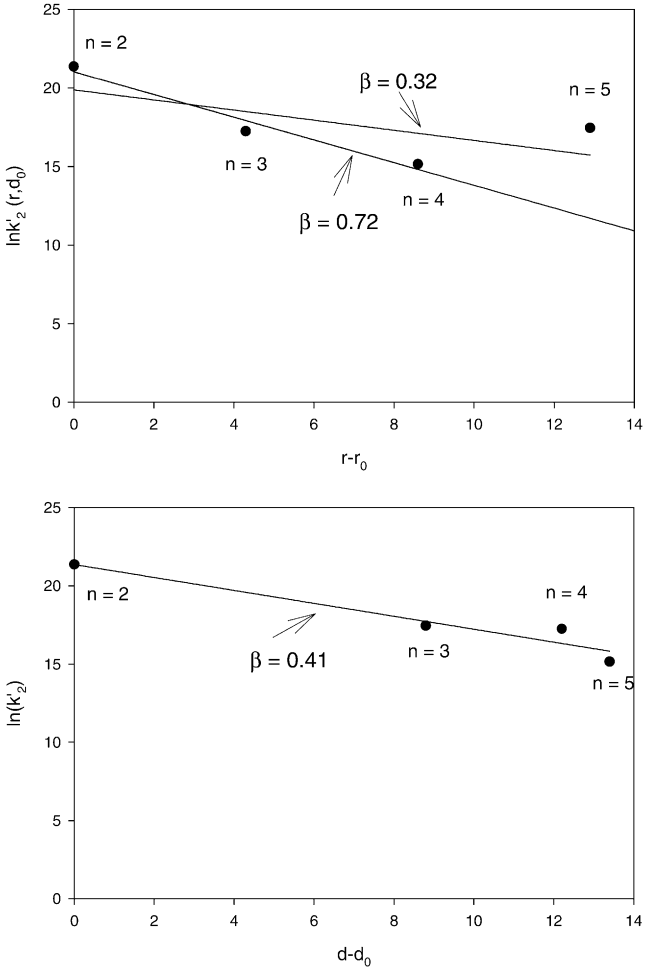

Fig. 17. Plots of $\ln k'_{ET}$ vs. through-bond ($r - r_0$) and through-space ($d - d_0$) distances in water at 25 °C. k'_{ET} is the electron transfer quenching rate constant corrected for the distance dependence of λ_0.

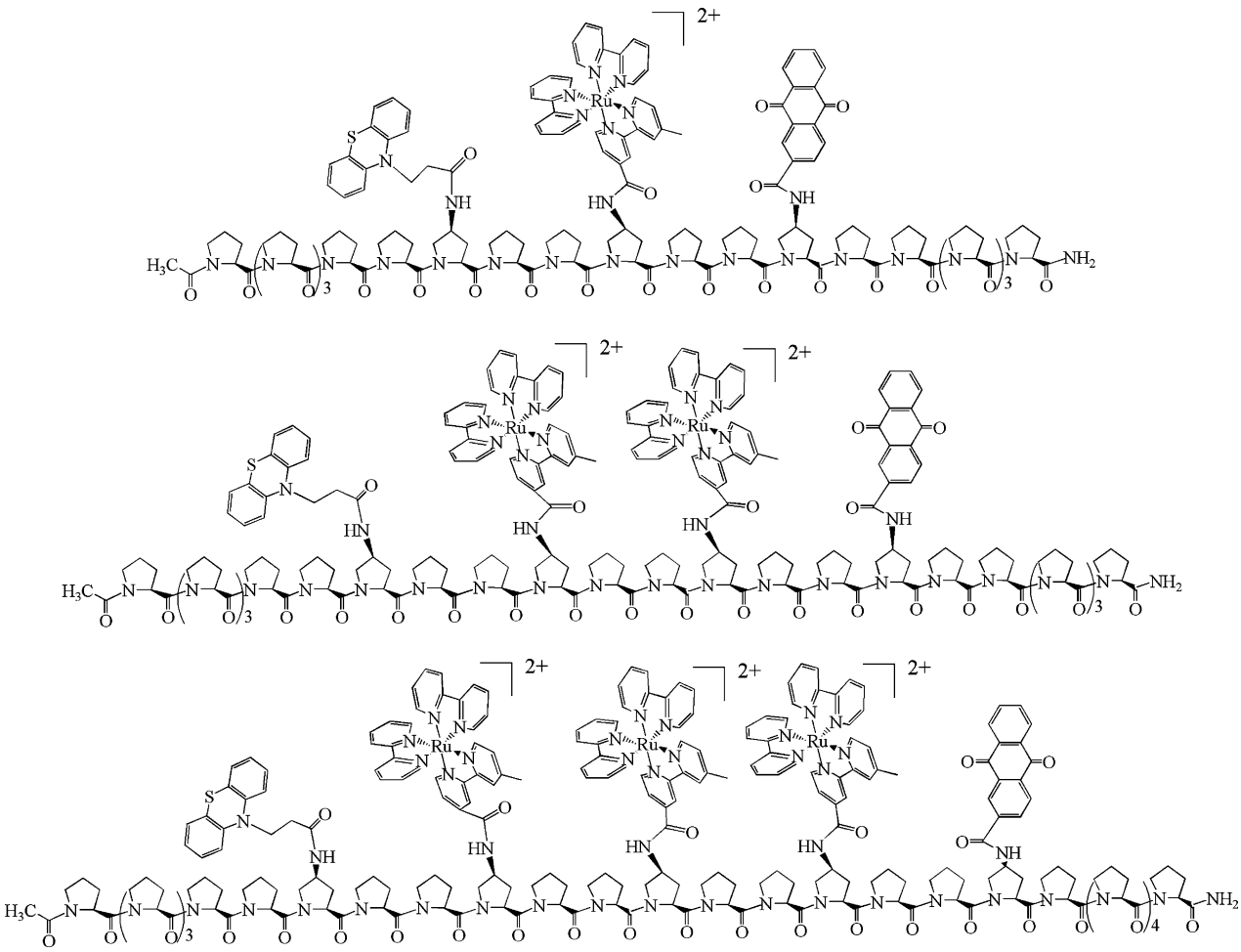

Fig. 18. Line structures of the antenna-electron transfer oligoproline arrays.

through-space electron transfer. With distances of this magnitude and through-space electron transfer, super-exchange coupling with the solvent and oligoproline scaffold no doubt play important roles in promoting electronic coupling [155].

Distance attenuation factors were evaluated from plots of $\ln k'_{ET}$ versus $d - d_0$ for both normal (β = 0.41) and inverted electron transfer (β = 0.48). The coincidence of the two values within experimental error is of fundamental significance. Electronic coupling is weak and electron transfer non-adiabatic in both cases. In both cases, reaction dynamics and the frequency factor for electron transfer are controlled by electron tunneling and the magnitude of H_{DA}.

If electronic coupling is strong, electron transfer is adiabatic and the transferring electron is in equilibrium with the coupled vibrational and solvent modes. In the inverted region or in excited state nonradiative decay, the dynamics of barrier crossing and frequency factor are dictated by the dynamics of vibrational modes that couple the initial and final electronic states and not by the extent of electronic coupling. With strong electronic coupling and adiabatic electron transfer in the normal region, barrier crossing dynamics are dictated by the slowest coupled nuclear motions. These are typically collective reorientational modes in the solvent.

5.3. Summary and conclusions

The oligoproline approach to molecular assemblies offers flexibility and synthetic versatility and, with proper design, facile intra-helix electron and energy transfer between appended functional groups. There is promise for adding catalytic sites to the Ru-bpy-based chromophore-electron transfer apparatus as a way of utilizing photochemically produced oxidative and reductive equivalents to drive irreversible reactions which is one of the goals of artificial photosynthesis [20,157].

The work described above was extended in two directions. In one, Fig. 18, the chromophore-donor–acceptor motif in oligoproline assemblies ZRA1 and ZRA2 was maintained as the number of intervening Ru(II)-bpy chromophores was increased from one to three [158].

This series was designed to explore the feasibility of imbedding an antenna-chromophore array within the PTZ–Anq quencher-electron transfer pair. The dynamical

studies described above showed that PTZ → Ru^{II*} quenching is efficient with $\tau \sim 20$–30 ns compared to the lifetime of the excited state of $\tau = 10^3$ ns. Anq quenching of Ru^{II*} is slow and inefficient. If energy migration across two proline spacers is sufficiently rapid, excitation at any of the Ru(II) chromophores in the assemblies with $n = 2$ or 3 would be followed by energy migration to the site adjacent to PTZ. The dynamical events would be similar to those described above for energy migration and transfer in [PS-$CH_2CH_2C(O)NH$-$(Ru^{II\prime})_{17}(Os^{II})_3$]$(PF_6)_{40}$. The results described above for assembly ZRRA showed that energy transfer is relatively slow across five pralines, but energy transfer across two spacers is rapid, see below. As in ZRRA, subsequent reductive electron transfer quenching and complex-to-complex electron migration by $bpy^{\bullet -}$ → bpy and $bpy^{\bullet -}$ → Anq electron transfer would create a RS state with a spatially separated $PTZ^{\bullet +}$–$Anq^{\bullet -}$ pair.

The second extension was related to the first and designed to explore the distance dependence of energy transfer. The same strategy was adopted as in the Ru(II)–PTZ distance dependence study but with Os(II) added as the energy acceptor as in the polymer-based assemblies.

The line structures of two oligoprolines in this series are shown in Fig. 18. All contain a Ru(II)–Ru(II)–Os(II) array with the number of proline spacers varied in the series n = 2, 3 (not shown), and 5. Initial steady-state and time-resolved experiments in CH_3CN reveal that Ru^{II*} → Os^{II} energy transfer, which is favored by 0.4 eV, is rapid for all three on the ns time scale. Energy migration by Ru(II)* → Ru(II) hopping is slower and clearly distance dependent [159].

Acknowledgements

Acknowledgements are made to the many co-workers whose efforts created this account and whose names appear in the references. In particular, I would like to acknowledge the highly productive collaborations with my faculty colleagues at the University of North Carolina including, David Whitten, Royce Murray, Bruce Erickson (deceased), Joe DeSimone, and John Papanikolas. We also acknowledge support of this research by the National Science Foundation, the Office of Basic Energy Sciences of the Department of Energy, and the Los Alamos National Laboratory.

References

[1] (a) J.N. Demas, A.W. Adamson, J. Am. Chem. Soc. 95 (1975) 5159;
(b) J.N. Demas, A.W. Adamson, J. Am. Chem. Soc. 93 (1971) 1800.
[2] H. Gafney, A.W. Adamson, J. Am. Chem. Soc. 94 (1972) 8238.
[3] C.R. Bock, T.J. Meyer, D.G. Whitten, J. Am. Chem. Soc. 96 (1974) 4710.
[4] R.C. Young, T.J. Meyer, D.G. Whitten, J. Am. Chem. Soc. 97 (1975) 4781.
[5] C.R. Bock, T.J. Meyer, D.G. Whitten, J. Am. Chem. Soc. 97 (1975) 2909.
[6] A.R. Gutierrez, T.J. Meyer, D.G. Whitten, Molec. Photochem. 7 (1976) 349.
[7] V. Balzani, F. Bolleta, M.T. Gandolfi, M. Maestri, Top. Curr. Chem. 75 (1978) 1.
[8] (a) N. Sutin, C. Creutz, Pure Appl. Chem. 52 (1980) 2717;
(b) N. Sutin, J. Photochem. 10 (1979) 19.
[9] (a) T.J. Meyer, Isr. J. Chem. 15 (1977) 200;
(b) T.J. Meyer, in: H. Malcolm, Chisholm (Eds.), Inorganic Chemistry: Toward the 21st Century, ACS Symposium Series, vol. 211, American Chemical Society, Washington, DC, 1983, p. 157.
[10] T.J. Meyer, in: S.J. Lippard (Ed.), Progress in Inorganic Chemistry, vol. 30, Wiley & Sons, New York, 1983, p. 389.
[11] C.R. Bock, J.A. Connor, A.R. Gutierrez, T.J. Meyer, D.G. Whitten, B.P. Sullivan, J.K. Nagle, J. Am. Chem. Soc. 101 (1979) 4815.
[12] C.R. Bock, J.A. Connor, A.R. Gutierrez, T.J. Meyer, D.G. Whitten, B.P. Sullivan, J.K. Nagle, Chem. Phys. Lett. 61 (1979) 522.
[13] J.K. Nagle, R.C. Young, T.J. Meyer, Inorg. Chem. 16 (1977) 3366.
[14] F.R. Keene, R.C. Young, T.J. Meyer, J. Am. Chem. Soc. 99 (1977) 2468.
[15] C.P. Anderson, D.J. Salmon, T.J. Meyer, R.C. Young, J. Am. Chem. Soc. 99 (1977) 1980.
[16] P.J. DeLaive, J.T. Lee, H.W. Sprintschnik, H. Abruna, T.J. Meyer, D.G. Whitten, J. Am. Chem. Soc. 99 (1977) 7094.
[17] R.C. Young, J.K. Nagle, T.J. Meyer, D.G. Whitten, J. Am. Chem. Soc. 100 (1978) 4773.
[18] A. Deronzier, T.J. Meyer, Inorg. Chem. 19 (1980) 2912.
[19] J.K. Nagle, T.J. Meyer, Inorg. Chem. 23 (1984) 3663.
[20] T.J. Meyer, Acc. Chem. Res. 22 (1989) 163.
[21] T.J. Meyer, Photoredox Catalysis, in: M. Tsutsui, R. Ugo (Eds.), Fundamental Research in Homogeneous Catalysis, Plenum Press, New York, 1977, p. 169.
[22] T.J. Meyer, in: J.R. Norris Jr., D. Meisel (Eds.), Energy Conversion at the Molecular Level in Photochemical Energy Conversion, Elsevier Science Publishing Co., Inc., New York, 1989, p. 75.
[23] B.P. Sullivan, H. Abruna, H.O. Finklea, D.J. Salmon, J.K. Nagle, T.J. Meyer, H. Sprintschnik, Chem. Phys. Lett. 58 (1978) 389.
[24] J.K. Nagle, J.S. Bernstein, R.C. Young, T.J. Meyer, Inorg. Chem. 20 (1981) 1760.
[25] J.C. Curtis, J.S. Bernstein, R.H. Schmehl, T.J. Meyer, Chem. Phys. Lett. 81 (1981) 48.
[26] T.J. Meyer, Photochemical electron transfer applied to the reduction of carbon dioxide carbon dioxide fixation and reduction in biological and model systems, in: C.-I. Brändén, G. Schneider (Eds.), Proceedings of the Royal Swedish Academy of Sciences, Nobel Symposia, Oxford University Press, 1994 (p. 211, Chaper 14).
[27] W.E. Jones Jr., S.M. Baxter, S.L. Mecklenburg, B.W. Erickson, B.M. Peek, T.J. Meyer, Supramol. Chem. Ser. C: Math. Phys. Sci. 371 (1992) 249.
[28] S.W. Gersten, G.J. Samuels, T.J. Meyer, J. Am. Chem. Soc. 14 (1982) 4029.
[29] R.A. Binstead, C.W. Chronister, J.F. Ni, C.M. Hartshorn, T.J. Meyer, J. Am. Chem. Soc. 122 (2000) 8464.
[30] B.P. Sullivan, M.R.M. Bruce, T.R. O'Toole, C.M. Bolinger, E. Megehee, H. Thorp, T.J. Meyer, in: W.M. Ayers (Ed.), Catalytic Activation of Carbon Dioxide American Chemical Society Symposium Series, vol. 363, American Chemical Society, Washington, DC, 1988 (p. 52, Chapter 6).
[31] J.R. Pugh, M.R.M. Bruce, B.P. Sullivan, T.J. Meyer, Inorg. Chem. 30 (1991) 86 (and references therein).
[32] T.J. Meyer, M.H.V. Huynh, Inorg. Chem. 42 (2002) 8140.

[33] (a) L. Hammarstrom, Curr. Opin. Chem. Biol. 7 (2004) 666;
(b) M. Hervas, J.A. Navarro, M.A. De La Rosa, Acc. Chem. Res. 36 (2003) 798.
[34] (a) S.D. Dai, K. Johansson, M. Miginiac-Maslow, P. Schurmann, H. Eklund, Photosyn. Res. 79 (2004) 233;
(b) H. Imahori, Y. Mori, Y. Matano, J. Photochem. Photobiol. C Photochem. Rev. 4 (2003) 51.
[35] C. Hicks, G.Z. Ye, C. Levi, M. Gonzales, I. Rutenburg, J.W. Fan, R. Helmy, A. Kassis, H.D. Gafney, Coord. Chem. Rev. 211 (2001) 207.
[36] T.J. Meyer, Pure Appl. Chem. 58 (1986) 1193.
[37] B.Z. Shan, Q. Zhao, N. Goswami, D.M. Eichhorn, D.P. Rillema, Coord. Chem. Rev. 211 (2001) 117.
[38] V. Balzani, A. Juris, Coord. Chem. Rev. 211 (2001) 97.
[39] J.J. Turner, M.W. George, F.P.A. Johnson, J.R. Westwell, Coord. Chem. Rev. 125 (1993) 101.
[40] P. Glyn, M.W. George, P.M. Hodges, J.J. Turner, J. Chem. Soc. Chem. Commun. (1989) 1655.
[41] J.R. Schoonover, C.A. Bignozzi, T.J. Meyer, Coord. Chem. Rev. 165 (1997) 239.
[42] K.M. Omberg, T.J. Meyer, J.R. Schoonover, in: S.G. Pandalai (Ed.), Recent Research Developments in Inorganic Chemistry, vol. 2, Transworld Research Network, India, 1999.
[43] (a) J.R. Schoonover, G.E. Strouse, Chem. Rev. 98 (1998) 1335;
(b) J.R. Schoonover, C.A. Bignozzi, T.J. Meyer, Coord. Chem. Rev. 165 (1997) 239;
(c) J.R. Schoonover, G.F. Strouse, K.M. Omberg, R.B. Dyer, Comm. Inorg. Chem. 18 (1996) 165.
[44] D.M. Dattelbaum, T.J. Meyer, in: T.J. Johnson, G. Zachman (Eds.), Step-Scan TRS Absorption Experiment of Organometallic Complexes: An Introduction to Step-Scan FTIR, Bruker Optics, Billerica, MA, 2000, p. 21.
[45] K.D. Demadis, C.M. Hartshorn, T.J. Meyer, Chem. Rev. 101 (2001) 2655.
[46] N.S. Hush, Prog. Inorg. Chem. 8 (1967) 391.
[47] N. Sutin, Adv. Chem. Phys. 106 (1999) 7.
[48] C. Creutz, M.D. Newton, N. Sutin, J. Photochem. Photobiol. A: Chem. 82 (1994) 47.
[49] K.M. Omberg, J.R. Schoonover, J.A. Treadway, R.M. Leasure, R.B. Dyer, T.J. Meyer, J. Am. Chem. Soc. 119 (1997) 7013.
[50] R.F. Dallinger, W.H. Woodruff, J. Am. Chem. Soc. 101 (1979) 4391.
[51] G.B. Shaw, C.L. Brown, J.M. Papanikolas, J. Phys. Chem. A 106 (2002) 1483.
[52] (a) J.P. Cushing, C. Butoi, D.F. Kelley, J. Phys. Chem. A 101 (1997) 7222;
(b) L.F. Cooley, P. Bergquist, D.F. Kelley, J. Am. Chem. Soc. 112 (1990) 2612.
[53] (a) J.L. Pogge, D.F. Kelley, Chem. Phys. Lett. 238 (1995) 16;
(b) R.A. Malone, D.F. Kelley, J. Chem. Phys. 95 (1991) 8970.
[54] D.M. Dattelbaum, E.M. Kober, T.J. Meyer, submitted.
[55] (a) H. Riesen, L. Wallace, E. Krausz, J. Chem. Phys. 102 (1995) 4823;
(b) H. Riesen, L. Wallace, E. Krausz, Int. Rev. Phys. Chem. 16 (1997) 291.
[56] L. Della Ciana, I. Hamachi, T.J. Meyer, J. Org. Chem. 54 (1989) 1731.
[57] T.D. Westmoreland, K.S. Schanze, P.E. Neveux Jr., E. Danielson, B.P. Sullivan, P. Chen, T.J. Meyer, Inorg. Chem. 24 (1985) 2596.
[58] T.D. Westmoreland, K.S. Schanze, P.E. Neveux Jr., E. Danielson, B.P. Sullivan, P. Chen, T.J. Meyer, Inorg. Chem. 24 (1985) 2596.
[59] J.C. Curtis, J.S. Bernstein, T.J. Meyer, Inorg. Chem. 24 (1985) 385.
[60] (a) T.J. Meyer, in: D. Vincenzo Balzani (Ed.), Supramolecular Photochemistry, Reidel Publishing Company, Dordrecht, Holland, 1987, p. 103 (Intramolecular Control of Light Induced Electron Transfer) ;
(b) T.J. Meyer, Pure Appl. Chem. 62 (1990) 1003.
[61] T.J. Meyer, Photochemical processes in organized molecular systems, in: X. Kenichi Honda (Ed.), Proceedings of the Memorial Conference for the late Professor Shigeo Tazuke, Yokohama, Japan, September 22–24, 1990, North-Holland, Elsevier, Amsterdam, 1991, p. 133 (Intramolecular, Photochemical Electron and Energy Transfer).
[62] E. Danielson, C.M. Elliott, J.W. Merkert, T.J. Meyer, J. Am. Chem. Soc. 109 (1987) 2519.
[63] J.A. Treadway, T.J. Rutherford, P.-Y. Chen, F.R. Keene, T.J. Meyer, J. Phys. Chem. B 101 (1997) 6824.
[64] E.H. Yonemote, G.B. Saupe, R.H. Schmehl, S.M. Hubig, R.L. Riley, B.L. Iverson, T.E. Mallouk, J. Am. Chem. Soc. 116 (1994) 4786.
[65] D.J. Styers-Barnett, E.J. Gannon, J.C. Granger, J.M. Papanikolas, S.W. Aldridge, J.R. Schoonover, D.M. Dattelbaum, T.J. Meyer, in press.
[66] N.H. Damrauer, G. Cerullo, A. Yeh, T.R. Boussie, C.V. Shank, J.K. McCusker, Science 275 (1997) 54.
[67] (a) N.H. Damrauer, B.T. Weldon, J.K. McCusker, J. Phys. Chem. A 102 (1998) 3382;
(b) N.H. Damrauer, J.K. McCusker, J. Phys. Chem. A 103 (1999) 8440.
[68] E. Danielson, C.M. Elliott, J.W. Merkert, T.J. Meyer, J. Am. Chem. Soc. 109 (1987) 2519.
[69] P.-Y. Chen, T.J. Meyer, Chem. Rev. 98 (1998) 1439.
[70] J.P. Claude, K.M. Omberg, D.S. Williams, T.J. Meyer, J. Phys. Chem. A 106 (2002) 7795.
[71] S. Boyde, G.F. Strouse, W.E. Jones Jr., T.J. Meyer, J. Am. Chem. Soc. 111 (1989) 7448.
[72] S.L. Mecklenburg, K.A. Opperman, P.-Y. Chen, T.J. Meyer, J. Phys. Chem. 100 (1996) 15145.
[73] J. Olmsted, T.J. Meyer, J. Phys. Chem. 91 (1987) 1649.
[74] C.M. Hartshorn, N. Daire, V. Tondreau, B. Loeb, T.J. Meyer, P.S. White, Inorg. Chem. 38 (1999) 3200.
[75] C.R. Arana, H.D. Abruña, Inorg. Chem. 32 (1992) 194.
[76] A. Gourdon, J.-P. Launay, Inorg. Chem. 37 (1998) 5336.
[77] C.M. Hartshorn, N. Daire, V. Tondreau, B. Loeb, T.J. Meyer, P.S. White, Inorg. Chem. 38 (1999) 3200.
[78] R.R. Ruminski, J. Kiplinger, T. Cockroft, C. Chase, Inorg. Chem. 28 (1989) 370.
[79] L.M. Vogler, K.J. Brewer, Inorg. Chem. 35 (1996) 818.
[80] C.M. Hartshorn, T.J. Meyer, unpublished results.
[81] C.N. Fleming, D.M. Dattelbaum, T.J. Meyer, in preparation.
[82] C.N. Fleming, L.M. Dupray, J.M. Papanikolas, T.J. Meyer, J. Phys. Chem. 106 (2002) 2328.
[83] C.N. Fleming, K.A. Maxwell, J.M. Papanikolas, T.J. Meyer, J. Am. Chem. Soc. 123 (2001) 10336.
[84] K.T. Wong, J.M. Lehn, S.M. Peng, G.H. Lee, Chem. Comm. 22 (2000) 2259.
[85] E. Galoppini, M.A. Fox, J. Am. Chem. Soc. 118 (1996) 2299.
[86] J.H. Clements, S.E. Webber, J. Phys. Chem. B 103 (1999) 9366.
[87] J.H. Clements, S.E. Webber, J. Phys. Chem. A 103 (1999) 2513.
[88] K. Schillén, A. Yekta, S. Ni, J.P.S. Farinha, M.A. Winnik, J. Phys. Chem. B 103 (1999) 9090.
[89] Y. Rharbi, A. Yekta, M.A. Winnik, R.J. DeVoe, D. Barrera, Macromolecules 32 (1999) 3241.
[90] K.A. Walters, L. Trouillet, S. Guillerez, K.S. Schanze, Inorg. Chem. 39 (2000) 5496.
[91] K.A. Walters, K.D. Ley, K.S. Schanze, Langmuir 15 (17) (1999) 5676.
[92] D.T. Mcquade, A.E. Pullen, T.M. Swager, Chem. Rev. 100 (2000) 2537.
[93] T.M. Swager, Acc. Chem. Res. 31 (1998) 201.
[94] L.X. Chen, W.J.H. Jäger, D.J. Gosztola, M.P. Niemczyk, M.R. Wasielewski, J. Phys. Chem. B 104 (2000) 1950.

[95] L.X. Chen, W.J.H. Jäger, M.P. Niemczyk, M.R. Wasielewski, J. Phys. Chem. A 103 (1999) 4341.
[96] E. Wolcan, G. Ferraudi, J. Phys. Chem. A 104 (2000) 9281.
[97] J.M. Calvert, J.V. Caspar, R.A. Binstead, T.D. Westmoreland, T.J. Meyer, J. Am. Chem. Soc. 104 (1982) 6620.
[98] R. Arshady, B.S.R. Reddy, M.H. George, Polymer 25 (1984) 716.
[99] L.D. Margerum, R.W. Murray, T.J. Meyer, J. Phys. Chem. 90 (1986) 728.
[100] R.E. Sassoon, J. Rabani, J. Phys. Chem. 89 (1985) 4710.
[101] J. Olmsted, S.F. McClanahan, E. Danielson, J.N. Younathan, T.J. Meyer, J. Am. Chem. Soc. 109 (1987) 3297.
[102] G.F. Strouse, L.A. Worl, J.N. Younathan, T.J. Meyer, J. Am. Chem. Soc. 111 (1989) 9101.
[103] W.E. Jones Jr., S.M. Baxter, G.F. Strouse, T.J. Meyer, J. Am. Chem. Soc. 115 (1993) 7363.
[104] J.N. Younathan, S.F. McClanahan, T.J. Meyer, Macromolecules 22 (1989) 1048.
[105] S.M. Baxter, W.E. Jones Jr., E. Danielson, L. Worl, G. Strouse, J. Younathan, T.J. Meyer, Coord. Chem. Rev. 111 (1991) 47.
[106] J.N. Younathan, W.E. Jones Jr., T.J. Meyer, J. Phys. Chem. 95 (1991) 488.
[107] L.A. Worl, G.F. Strouse, J.N. Younathan, S.M. Baxter, T.J. Meyer, J. Am. Chem. Soc. 112 (1990) 7571.
[108] L.A. Worl, W.E. Jones, G.F. Strouse, J.N. Younathan, E. Danielson, K.A. Maxwell, M. Sykora, T.J. Meyer, Inorg. Chem. 28 (1999) 2705.
[109] L.M. Dupray, T.J. Meyer, Inorg. Chem. 35 (1996) 6299.
[110] L.M. Dupray, M. Devenney, D.R. Striplin, T.J. Meyer, J. Am. Chem. Soc. 119 (1997) 10243.
[111] J.K. Nagle, R.C. Young, T.J. Meyer, Inorg. Chem. 16 (1997) 3366.
[112] C.N. Fleming, L.M. Dupray, J.M. Papanikolas, T.J. Meyer, J. Phys. Chem. 106 (2002) 2328.
[113] S.L. Mecklenburg, B.M. Peek, J.R. Schoonover, D.G. McCafferty, C.G. Wall, B.W. Erickson, T.J. Meyer, J. Am. Chem. Soc. 115 (1993) 5479.
[114] G.D. Smith, K.A. Maxwell, J.M. DeSimone, T.J. Meyer, R.A. Palmer, Inorg. Chem. 39 (2000) 893.
[115] C.N. Fleming, L.M. Dupray, J.M. Papanikolas, T.J. Meyer, J. Phys. Chem. 106 (2002) 2328.
[116] E.M. Kober, T.J. Meyer, Inorg. Chem. 21 (1982) 3967.
[117] E.M. Kober, J.V. Caspar, R.S. Lumpkin, T.J. Meyer, J. Phys. Chem. 90 (1986) 3722.
[118] Z. Murtaza, D.K. Graff, A.P. Zipp, L.A. Worl, W.E. Jones Jr., W.D. Bates, T.J. Meyer, J. Phys. Chem. 98 (1994) 10504.
[119] D. Graff, J.P. Claude, T.J. Meyer, in: S. Isied (Ed.), Advances in Chemistry 253, American Chemical Society, Washington, DC, 1997 (Chapter 11).
[120] K.M. Omberg, P.Y. Chen, T.J. Meyer, in: J. Jortner, M. Bixon (Eds.), Advances in Chemical Physics Series 106, Wiley & Sons, New York, 1998 (Chapter 11).
[121] S. Speiser, Chem. Rev. (1996) 96.
[122] M. Sykora, K.A. Maxwell, J.M. DeSimone, T.J. Meyer, Proc. Natl. Acad. Sci. USA 97 (2000) 7687.
[123] (a) S. Nakahama, A. Hirao, Prog. Polym. Sci. 299 (1990);
(b) K. Susuki, A. Hirao, S. Nakamana, Makromol. Chem. 190 (1989) 2893.
[124] D.A. Friesen, T. Kajita, T.J. Meyer, Inorg. Chem. 37 (1998) 2756.
[125] R.M. Leasure, T. Kajita, T.J. Meyer, Inorg. Chem. 35 (1996) 5962.
[126] C.N. Fleming, K.A. Maxwell, J.M. Papanikolas, T.J. Meyer, J. Am. Chem. Soc. 123 (2001) 10336.
[127] M.A. Peters, A.M. Belu, R.W. Linton, L. Dupray, T.J. Meyer, J.M. DeSimone, J. Am. Chem. Soc. 117 (1995) 3380.
[128] P. Chen, K.M. Omberg, D.A. Kavaliunas, J.A. Treadway, R.A. Palmer, T.J. Meyer, Inorg. Chem. 36 (1997) 954.
[129] K.M. Omberg, T.J. Meyer, J.R. Schoonover, Inorg. Chem. 39 (2000) 69.
[130] M. Sykora, T.J. Meyer, Chem. Mater 11 (1999) 1186.
[131] M. Sykora, K.A. Maxwell, T.J. Meyer, Inorg. Chem. 38 (1999) 3596.
[132] I. Rubinstein, C.R. Martin, A.J. Bard, Anal. Chem. 55 (1983) 1580.
[133] C.N. Fleming, J.M. Papanikolas, T.J. Meyer, in preparation.
[134] P.-Y. Chen, E. Danielson, T.J. Meyer, J. Phys. Chem. 92 (1988) 3708.
[135] C.N. Fleming, P. Jang, T.J. Meyer, J.M. Papanikolas, J. Phys. Chem. B 108 (2004) 2205.
[136] A.D. Stein, K.A. Peterson, M.D. Fayer, J. Chem. Phys. 92 (1990) 5622.
[137] M. Devenney, L.A. Worl, S. Gould, A. Guadalupe, B.P. Sullivan, J.V. Caspar, R.L. Leasure, J.R. Gardner, T.J. Meyer, J. Phys. Chem. 101 (1997) 4535.
[138] B.M. Peek, S.E. Vitols, T.J. Meyer, B.W. Erickson, in: J.E. Rivier, G.R. Marshell (Eds.), Peptides: Chemistry, Structure and Biology, ESCOM, Leiden, 1990, p. 1076.
[139] B.M. Peek, S.W. Edwards, S.L. Mecklenburg, T.J. Meyer, B.W. Erickson, in: J.A. Smith, J.E. Rivier (Eds.), 12th American Peptide Symposium, Escom, Leiden, Netherlands, 1991, p. 462.
[140] D.G. McCafferty, B.M. Bishop, C.G. Wall, S.G. Hughes, S.L. Mecklenberg, T.J. Meyer, B.W. Erickson, Tetrahedron 51 (1995) 1093.
[141] S.L. Mecklenburg, B.M. Peek, B.W. Erickson, T.J. Meyer, J. Am. Chem. Soc. 113 (1991) 8540.
[142] S.L. Mecklenburg, B.M. Peek, J.R. Schoonover, D.G. McCafferty, C.G. Wall, B.W. Erickson, T.J. Meyer, J. Am. Chem. Soc. 115 (1993) 5479.
[143] S.L. Mecklenburg, D.G. McCafferty, J.R. Schoonover, B.M. Peek, B.W. Erickson, T.J. Meyer, Inorg. Chem. 33 (1994) 2974.
[144] B.W. Erickson, R.B. Merrifield, Proteins 2 (1976) 255.
[145] S.S. Isied, A.A. Vassalian, R.H. Magnuson, H. Schwartz, J. Am. Chem. Soc. 107 (1985) 7432.
[146] K.S. Schanze, K. Sauer, J. Am. Chem. Soc. 110 (1988) 1180.
[147] K.S. Schanze, L.A. Cabana, J. Phys. Chem. 94 (1990) 2740.
[148] M.Y. Ogawa, I. Moreira, J.F. Wishart, S.S. Isied, Chem. Phys. 176 (1993) 589.
[149] D.G. McCafferty, D.A. Friesen, E. Danielson, C.G. Wall, M.J. Saederholm, B.W. Erickson, T.J. Meyer, Proc. Natl. Acad. Sci. USA 93 (1993) 8200.
[150] C. Slate, R. Binstead, T.J. Meyer, B.W. Erickson, Lett. Pept. Sci. 6 (1999) 61.
[151] D.R. Striplin, S.Y. Reece, D.G. McCafferty, C.G. Wall, D.A. Friesen, B.W. Erickson, T.J. Meyer, J. Am. Chem. Soc. 126 (2004) 5282.
[152] P. Gilch, F. Pollinger-Dammer, C. Musewald, U.E. Steiner, M.E. Michel-Beyerle, Science 281 (1998) 982.
[153] T. Klumpp, M. Linsenmann, D. Burssner, E.B. Krissinel, S.L. Larson, C.M.S. Elliott, U.E. Steiner, J. Am. Chem. Soc. 121 (1999) 1076.
[154] C.A. Slate, D.R. Striplin, J.A. Moss, P.-Y. Chen, B.W. Erickson, T.J. Meyer, J. Am. Chem. Soc. 120 (1998) 4885.
[155] S.A. Serron, S.A. Aldridge III, C.N. Fleming, R.M. Danell, M.-H. Baik, M. Sykora, D.M. Dattelbaum, T.J. Meyer, in press.
[156] J.P. Claude, T.J. Meyer, J. Phys. Chem. 99 (1995) 51.
[157] C.M. Hartshorn, K.A. Maxwell, P.S. White, J.M. DeSimone, T.J. Meyer, Inorg. Chem. 40 (2001) 601.
[158] S.A. Serron, S.A. Aldridge III, R.M. Danell, T.J. Meyer, Tetrahedron Lett. 41 (2000) 4039.
[159] S.A. Aldridge, S.A. Serron, C.N. Fleming, unpublished results.